Multi-mode Quantum Synchronization

Lotte van Dongen

11th July 2018

Delft University of Technology
Bachelor of Applied Physics and Applied Mathematics
Supervisors: Dr. J.L.A. Dubbeldam and Prof. Dr. Y.M. Blanter

Abstract

The dynamics of interacting many-particle systems on quantum mechanical scale is a broad subject of research in modern physics. The understanding of the quantum correlations, or entanglement, between the particles in an isolated many-body quantum system may however be challenging, as the amount of interactions may be large. To be able to describe the system in a simpler way, mean field theory is often applied; the interactions of all individual particles are substituted by an averaged effect.

First and second order mean field approximations are applied to the equations of motion of the amplitudes $c_n = \langle \hat{a}_n \rangle$ for each mode of the many-body system. In first order mean field, under the assumption that each mode has the same magnitude of the (constant) amplitude, the Kuramoto equation follows for the phases of the complex amplitudes [1]. To study this first order approximation and to refine the mean field solution, the equations of motion have been extended to second order mean field.

After that, numerical integration is used to solve the system of coupled differential equations for two modes. The solutions seem unstable, which is verified by defining quantum fluctuations beyond mean field. These are shown not to be negligible for a two mode system.

It was discovered that the mean field equations of motion show divergent fluctuations for a system of two modes, which opens a whole set of questions on the validity of the first order mean field approximation and therefore the use of the Kuramoto model for quantum many-body dynamics. The extension to the second order mean field solutions might be promising as this does include correlations between the operators.

Contents

1 Introduction

The world around us consists of interacting many-particle systems. The dynamics of these systems on quantum mechanical scale is a broad subject of research in modern physics. Quantum many-body theory (for example condensed matter physics or statistical mechanics) could be seen as the essential link between entanglement theory and quantum computing [40, 15]. The correlations that originate from coherent interaction between a large number of constituents are present in both quantum many-body models describing natural systems or materials as well as the physical systems that are built in laboratories to realize quantum information processing [15].

The understanding of the quantum correlations, or entanglement, between the particles within the system may however be challenging. Namely, in a system consisting of a large number of particles, the amount of interactions will be large. Hilbert space grows exponentially with the number of particles due to entanglement [23]. Therefore, the wave function which describes the state of the total system holds a lot of information and might be very impractical to work with. Systems with non-trivial interactions are impossible to treat fully analytically [41]. To be able to describe the many-body system, one often approximates the interactions of all individual particles with an averaged effect. This is known as mean field theory, and is applied often in condensed matter physics. Another approach to describe the complex system is to use perturbation theory; one takes the exact solution of a simpler system as a starting point and perturbs this system by introducing a small disturbance [20, 41].

This thesis is based on the article "Classical synchronization indicates persistent entanglement in isolated quantum systems" by *Dirk Witthaut et al.* [1]. This article, published in Nature in April 2017, concerns a relatively new topic in physics which lives on the boundary of two different subjects; classical synchronization and quantum entanglement. Collective phenomena of the classical and the quantum realms were previously seen as two distinct subjects with their own mathematical description and physical behaviour. In this paper however, a connection was shown between classical synchronization and entanglement in the earlier discussed quantum many-body systems. The results showed that it is possible to describe a quantum many-body system like the Bose-Einstein condensate with the relatively simple Kuramoto model. Both mean field and perturbation theory were used to find and assess the Kuramoto equations as a means to express entanglement as classical synchronization.

In this thesis, the link between the Kuramoto model for classical synchronization and quantum entanglement is explained in detail. In order to do so, knowledge on both the Kuramoto model and quantum field dynamics or quantum optics is needed. In the derivation of the Kuramoto equations for the quantum many-body system, first order mean field theory is applied in *Witthaut et al.* [1]. The goal of this research is to examine this approximation and to apply second order mean field to approach the theoretical exact solution more closely. The coupled differential equations that are found to describe the system in second order mean field are solved numerically, as they are non-linear and therefore cannot be solved analytically. The results showed that for two modes only, the mean field approximation gives unstable solutions. To confirm this, equations for the quantum fluctuations beyond mean field are derived using perturbation theory.

As the results for the second order mean field solutions were unstable for two modes, a natural continuation of this research would be to expand the numerical solutions to a higher number of modes. This way, the theoretically more accurate equations can be checked and their influence can be tested.

The theoretical background needed to derive the Kuramoto model for the quantum-many body systems will be discussed in Sections 2 and 3. In Section 3.4 the first order mean field approximation is used to derive the equations of motion for the quantum many-body system. To this point, all results were found in earlier research. In Section 4, the newly found results will be discussed. Section 4.1 gives the derivation of the differential equations for second order mean field. For both first and second order mean field, the coupled differential equations are solved numerically for two modes. These results are discussed in Section 4.2. The stability of the solutions is further examined in Section 4.3. Finally, the concluding remarks are presented in Section 5.

2 Classical Synchronization - the Kuramoto Model

Synchronization is a phenomenon which shows in many different forms, and is therefore studied in many fields of science [8]. In physical and technological applications and research, it shows in for example power, sensor and communication networks [13] as well as in coupled lasers [26] or Josephson junctions [37]. In biology and social sciences, synchronization plays an important role in neurology but can also be applied to opinion or voting dynamics [8].

As synchronization is such a fundamental principle, applicable in many fields and situations, it might be difficult to express the fundamental phenomenon mathematically. In the 1970s, Yoshiki Kuramoto proposed a model to describe the behaviour of a large set of coupled oscillators which may or may not synchronize [2]. This model was mathematically simple enough to be easily solvable, but at the same time it was very universally applicable and showed a large variety of synchronization patterns. Therefore, it is now a celebrated model for a large range of synchronization problems.

The Kuramoto Model is thus used to describe (classical) synchronization networks. It describes the behaviour of a large set of N coupled phase oscillators, $\theta_i(t)$, which have a natural frequency ω_i. These frequencies are drawn from the (possibly unknown) frequency distribution $g(\omega)$. Intuitively, the situation is as follows. Each oscillator tends to move independently at its own natural frequency, but the coupling between the oscillators forces them to synchronize with each other. The dynamics of these coupled oscillators can be described by the following differential equation [2, 8, 12, 27]

$$\frac{d\theta_i}{dt} = \omega_i + \sum_{j=1}^{N} K_{ij} \sin(\theta_j - \theta_i), \quad i = 1, 2..., N \tag{2.1}$$

In this equation, the coupling between each oscillator is described by the second term. Oscillator i is influenced by all other $N-1$ oscillators sinusoidally, with coupling parameter K_{ij}. This parameter is a measure for the extend to which the two oscillators interact. When the coupling is sufficiently weak, all oscillators will run incoherently. Beyond a certain threshold, synchronization emerges spontaneously and the oscillators will move collectively.

The assumptions that have to be made in order for this model to describe the system accurately are as follows [2]. Firstly, the oscillators all have to be (nearly) identical. This ensures that each oscillator influences the other in a similar manner. Furthermore, the interactions between the oscillators have to depend sinusoidally on the phase difference between each pair. This is often the case in physical systems, for example for a simple pendulum. In this case, the interaction is periodic and the contribution must be zero if the phases are the same.

As the Kuramoto model constitutes a set of N coupled non-linear differential equations, it is not trivially solvable analytically. When the oscillators are assumed to have mean field coupling, the equations can indeed be solved analytically [2, 8]. In the next section, this assumption will be introduced. Its analytical solutions will be presented in Sections 2.1.1, 2.1.2 and 2.1.3.

2.1 Mean Field Coupling

Mean field coupling can be seen as a simplification of the Kuramoto model, in which the differential equations can be solved analytically under the assumption of infinitely many oscillators. In mean field coupling, the coupling is all to all and constant. This means that each oscillator will feel a contribution from all other oscillators of the same strength , given that they have the same phase difference. This can be implemented in the Kuramoto model by choosing the coupling parameter K_{ij} to be a constant for all combinations of i and j. For example, let $K_{ij} = K/N > 0$. In this case, the coupling constant can be put in front of the summation in the original differential equation (2.1). The behaviour of a large set of individual oscillators is studied by the replacing it with a simpler model, in which the effect of all other oscillators on one particular oscillator is approximated by a single averaged effect [2, 8].

The mean field limit of the Kuramoto model for network synchronization can be solved analytically for infinitely many oscillators, thus for $N \to \infty$ [2, 8, 42]. After a transformation to a different set of coordinates, the problem reduces to a system of independent differential equations. The solutions for this problem can be divided into three types; the incoherent solution, global synchronization and solutions for partial synchronization. These solutions will be discussed separately in Sections 2.1.1, 2.1.3 and 2.1.2 respectively. The derivation of these solutions is explained very clearly by *Acebrón et al.* [2] and will be discussed briefly.

Firstly, a transformation can be made to the order parameter R, defined as in equation (2.2). This parameter will take a value in the complex plane in such a way that it describes the average effect of the system on one oscillator.

$$R = \frac{1}{N} \sum_{j=1}^{N} e^{i\theta_j} \tag{2.2}$$

This parameter can be rewritten as $R = re^{i\phi}$. This way, r is a measure of the phase coherence, whereas ϕ is the average phase of all oscillators. In Figure 1, these descriptions are visualized. The oscillators are represented by particles moving on the unit circle in the complex plane. Their phase θ_i is represented by the angle at which they are positioned. The order parameter $R = re^{i\phi}$ is visualized by the blue arrow. The measure of phase coherence $r{=}|R|$ can thus be deduced from the length of the arrow. The average phase $\phi = \arg(R)$ is shown by the angle of the arrow. The left picture shows scattered phases, in which case r is small. The oscillators are therefore not synchronized. The right picture shows clumped phases, in which case r is large. If this is the case for the equilibrium, thus for long times, the system is shown to be synchronized [28].

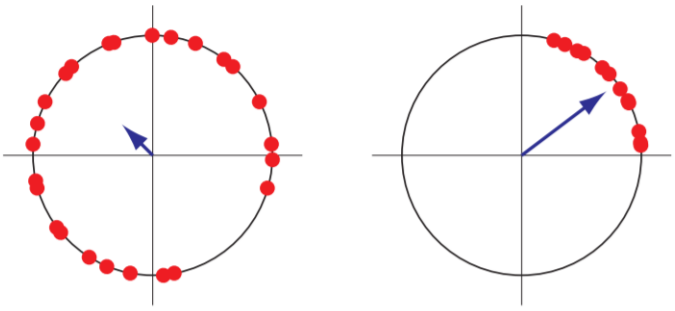

Figure 1: Visualization of oscillators moving on the unit circle, represented by the red dots, and the corresponding order parameter R, shown with the blue arrow. The left and right images show a non-synchronized and a synchronized system respectively [28].

In this parameter transformation, the mean field approximation is visible very clearly; the influence of all oscillators on one particular oscillator is replaced by the average influence that they generate together.

When the definitions of these order parameters are implemented in the Kuramoto equation (2.1), it reduces to

$$\frac{d\theta_i}{dt} = \omega_i + Kr\sin(\phi - \theta_i), \quad i = 1, 2, ..., N \tag{2.3}$$

In this equation, the order parameters r and ϕ are time-dependent and thus govern the dynamical behaviour. Note that the oscillators' equations are no longer explicitly coupled. From this equation, it can be noticed that each oscillator is coupled to the average phase with a coupling strength of Kr. The phase of an oscillator is thus pulled towards the mean phase ϕ, as might be expected. Furthermore, the strength of the coupling is proportional to the coherence r. This means that the behaviour includes positive feedback; the higher the coherence, the larger the coupling strength which will once again lead to a higher coherence.

The order parameter $R = re^{i\phi}$ can be rewritten into a continuous integral over $d\theta$ in the following way

$$re^{i\phi} = \int_{-\pi}^{\pi} e^{i\theta}\left(\frac{1}{N}\sum_{j=1}^{N}\delta(\theta - \theta_j)\right)d\theta \tag{2.4}$$

In definition (2.2), and thus in equation (2.4), the mean over all oscillators was calculated in a discrete way with a summation. However, the oscillators may be expected to be distributed with a probability density $\rho(\theta, t|\omega)$ in the limit of infinitely many oscillators. This probability density describes the density of these oscillators for each phase θ and time t for given frequency ω. The frequencies can be described with a distribution as well. Therefore, this mean becomes an average over phase and frequency in the following way

$$re^{i\phi} = \int_{-\pi}^{\pi}\int_{-\infty}^{\infty} e^{i\theta}\rho(\theta, t|\omega)g(\omega)d\theta d\omega \tag{2.5}$$

This equation can only be solved if the density distribution function $\rho(\theta, t|\omega)$ is determined, as the frequency distribution $g(\omega)$ is already given. To find this density distribution ρ, a continuity

equation can be defined for the oscillator density [2, 8, 27]

$$\frac{\partial \rho}{\partial t} + \frac{\partial}{\partial \theta}[\rho v] = 0 \tag{2.6}$$

In this equation, v is the angular or drift velocity of the oscillators defined as (2.7), in accordance with equation (2.3) [2].

$$v = \omega + Kr\sin(\phi - \theta) \tag{2.7}$$

This gives the following continuity equation.

$$\frac{\partial \rho}{\partial t} + \frac{\partial}{\partial \theta}\Big([\omega + Kr\sin(\phi - \theta)]\rho\Big) = 0 \tag{2.8}$$

The set of equations (2.5), (2.8) and the normalization condition (2.9) can be now be solved with an initial condition [2, 8].

$$\int_{-\pi}^{\pi} \rho(\theta, t|\omega) d\theta = 1 \tag{2.9}$$

In the following sections, the solutions to this set of equations will be discussed.

2.1.1 Incoherent Solution

The first solution is the trivial solution to the set of equations (2.5), (2.8) and (2.9), namely the uniform distribution

$$\rho(\theta, t|\omega) = \frac{1}{2\pi} \tag{2.10}$$

along with the phase coherence $r = 0$. This corresponds to a uniform angular distribution on the interval $[-\pi, \pi]$. In this steady-state solution, the oscillators run independently and incoherently [2, 8].

A different way to find this solution is the following. If the coupling parameter is assumed to go to zero, $K \to 0$, the differential equation (2.3) reduces such that the coupling term is left out. The solution for the phase then becomes

$$\theta_i(t) = \omega_i t + \theta_i(0) \tag{2.11}$$

This solution matches with the intuitive effect; when the coupling becomes very weak and can be neglected, each oscillator will rotate at its own natural angular frequency. If $\theta = \omega t$ is inserted in equation (2.5) and we let $t \to \infty$, it follows that the double integral goes to zero by the Riemann-Lebesgue lemma [6]. [1] This results in $r \to 0$, which is in accordance with the fact that the order parameter can be seen as a measure of the coherence of the population. The oscillators do not synchronize, thus their coherence approaches zero [2].

Theoretically, this solution results in Figure 2 if we plot the measure of phase coherence $r = |R|$ (definition 2.2) versus the time [28]. The phase coherence will decrease to zero as all oscillators will move at their own natural frequency.

[1] The Riemann-Lebesgue lemma says that the Fourier transform or Laplace transform of an L^1 function vanishes at infinity: $\hat{f}(z) := \int f(x)e^{-iz\cdot x}dx \to 0$ as $|z| \to \infty$

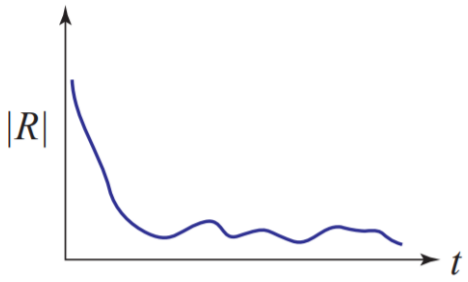

Figure 2: Theoretical plot of the magnitude of the order parameter $|R| = r$ versus time t with weak coupling [28]. This plot mainly serves to see the intuitive effect of a small coupling coupling parameter to the behaviour of the order parameter in time and is based on the numerical plot with $K = 0.1$ and $N = 256$ in [28].

2.1.2 Partial Synchronization

The second solution to the set of equations (2.5), (2.8) and (2.9) can be found under the following assumption

$$\frac{\partial \rho(\theta, t|\omega)}{\partial t} = 0 \tag{2.12}$$

The continuity equation (2.6) then implies

$$\frac{\partial}{\partial \theta}[\rho v] = 0 \tag{2.13}$$

Thus, the product of the oscillators' probability distribution and the angular velocity is constant in θ. $C(\omega)$ can be introduced to describe ρv [2, 9]. The behaviour of the oscillators can now be split up into two categories, based on this parameter $C(\omega)$. If $C(\omega) = 0$, the oscillators will be locked in synchronization. For a non-zero value of this variable, the oscillators will move incoherently at their own natural frequency. These two domains will be discussed briefly, such that the derivation is clear. For more details, see [2, 8, 9, 42].

If on the one hand $\rho v = C(\omega) = 0$, the normalization condition (2.9) forces the drift velocity v to be zero. Namely, the probability distribution may not be constantly zero, as this would not satisfy the normalization condition (2.9). A zero drift velocity implies

$$Kr \sin(\phi - \theta) = \omega \tag{2.14}$$

An oscillator moving at at its own drift velocity v_i will become stably locked at an angle such that (2.14) holds and $\frac{-\pi}{2} \leq (\theta - \phi) \leq \frac{\pi}{2}$ [2]. The oscillators will then be locked for some frequencies only, depending on the coupling parameter K and the coherence r. Oscillators with frequencies satisfying

$$|\omega| < Kr \tag{2.15}$$

can be locked and will synchronize [2, 8, 9]. This can be shown by determining the Jacobi matrix of the system.

On the other hand, all oscillators with frequencies $|\omega| > Kr$ cannot be locked in phase with the

synchronized oscillators. For these oscillators, (2.14) will never be satisfied, therefore $C(\omega) \neq 0$. The normalization condition (2.9) gives

$$C(\omega) = \frac{1}{2\pi}\sqrt{\omega^2 - (Kr)^2} \tag{2.16}$$

The expression for the density of oscillators becomes [2, 9, 42]

$$\rho(\theta, t|\omega) = \frac{C(\omega)}{v} = \frac{C(\omega)}{|\omega - Kr\sin(\theta - \phi)|} \tag{2.17}$$

This means the density is inversely proportional to the speed. This is in accordance with the intuitive expectations; one would expect most populated places (with high density) to have a drift which is more slowly, and in very free places (with low density) the flow can be fast.

In conclusion, partial synchronization results in the following stationary density [2]

$$\rho(\theta, t|\omega) = \begin{cases} \delta\big(\theta - \phi - \sin^{-1}\big(\frac{\omega}{Kr}\big)\big)H(\cos(\theta)) & |\omega| < Kr \\ \frac{C(\omega)}{|\omega - Kr\sin(\theta-\phi)|} & \text{elsewhere} \end{cases} \tag{2.18}$$

with $H(x)$ the Heaviside unit step function.

Now, the order parameter is evaluated by substituting the found density in equation (2.5) [2]. [2]. The final equation for the order parameter results in

$$r = Kr\int_{-\pi/2}^{\pi/2} \cos^2(\theta) g(Kr\sin(\theta))d\theta \tag{2.19}$$

Clearly, the trivial solution is $r = 0$, which again corresponds with the incoherently moving oscillators. Furthermore, it has a branch of solutions that correspond to the partially synchronized phase. These solutions must satisfy

$$1 = K\int_{-\pi/2}^{\pi/2} \cos^2(\theta) g(Kr\sin(\theta))d\theta \tag{2.20}$$

This branch bifurcates continuously from $r = 0$ at the critical value for the coupling parameter $K = K_c$ [2]. If we set $r = 0$ in equation (2.20) the critical coupling parameter is found.

$$K_c = \frac{2}{\pi g(0)} \tag{2.21}$$

Above this critical coupling parameter, synchronization will occur. This means that the oscillators which satisfy $|\omega| < Kr$ will be locked, whereas the others will move out of synchrony. The measure of phase coherence $r = |R|$ (definition 2.2) for the total system will be between zero and one, and is dependent on the number of oscillators which satisfy equation (2.15) with $K > K_c$ of equation (2.21).

[2]The derivation of this integral can be found in *Acebrón et al.* Two assumptions have to be made in order to find the proper result. Firstly, the frequency distribution function is even, thus $g(\omega) = g(-\omega)$. Secondly, the density function is symmetric such that $\rho(\theta + \pi| - \omega) = \rho(\theta|\omega)$.

2.1.3 Global Synchronization

In the limit of strong coupling, $K \to \infty$, all oscillators will be synchronized to their average phase ϕ. This results in total synchronization; all oscillators will move at the same frequency ω and phase $\theta_i = \phi$ for all i. Therefore, the phase coherence will be maximal, which results in $r = 1$.

Where the full and partial synchronization solutions could be found from the differential equations (2.5), (2.8) and (2.9), this is not possible for the global synchronization solution. This is due to the fact that these equations can only be solved for finite values of K. Therefore, the global synchronization solution is a limit of the partial synchronization, namely for large K.

In Figure 3, the theoretical plot of the measure of phase coherence $r = |R|$ (definition 2.2) versus time for strong coupling [28]. The phase coherence will increase to one as all oscillators will synchronize.

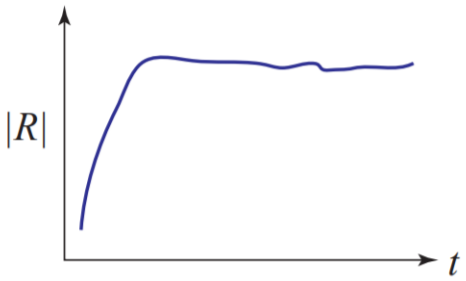

Figure 3: Theoretical plot of the magnitude of the order parameter $|R| = r$ versus time t with strong coupling [28]. This plot mainly serves to see the intuitive effect of a large coupling coupling parameter to the behaviour of the order parameter in time and is based on the numerical plot with $K = 0.5$ and $N = 256$ in [28].

2.1.4 Conclusions and Stability

In conclusion, we have seen that we can solve Kuramoto's model for an infinite number of oscillators in the mean field limit. By transferring to the coordinate system of the order parameters r (a measure of the phase coherence) and ϕ (the average phase), three types of solutions can be found. The incoherent solution shows total incoherence, in the absence of any coupling between the oscillators. Partial synchronization occurs for non-zero coupling parameters and implies that only part of the oscillators will synchronize. Namely, those which are in the interval $|\omega| < Kr$. Lastly, in the limit of infinitely strong coupling, all oscillators will synchronize and move together.

Note that all derivations and solutions in the above Sections 2.1.1, 2.1.2 and 2.1.3, hold only for the limit of infinitely many oscillators or $N \to \infty$.

For infinitely many oscillators, partial synchronization will occur for values of the coupling parameter of $K_c < K < \infty$. This results in values of the order parameter $0 < r < 1$. For $K < K_c$, the incoherent solution is found, which gives $r = 0$. Only for $K \to \infty$, total synchronization will occur in which all oscillators have locked together and move at the same frequency. In this case, the phase coherence is maximal, indicated by $r = 1$.

As noted before, the differential equations cannot be solved this way for a finite number of

oscillators. One can conclude however, that in this case there is no critical coupling parameter that indicates a (discontinuous) critical point before which no oscillators synchronize [2]. Furthermore, only partial synchronization will occur if $N \neq \infty$. This can be seen from the definition of the order parameter (2.2). Only for an infinite number of oscillators the order parameter will be zero.

The solutions that may occur in a real system will therefore always be partial synchronization. The system includes both some synchronized oscillators (as the coupling parameter is non-zero) and some non-synchronized oscillators (as the coupling parameter is not infinitely large). In other words, several oscillators will be phase-locked and will move together with constant frequency. The others will rotate out of synchrony with the locked oscillators.

The conclusions above for the solutions for either a finite or infinite number of oscillators are visualised in Figure 4 [3] and Table 1.

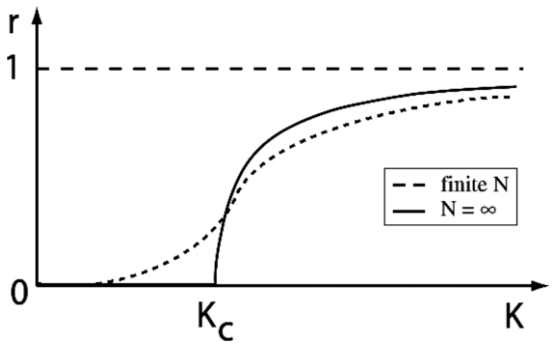

Figure 4: Theoretical plot of the magnitude of the order parameter $|R| = r$ versus coupling strength K, for infinitely many oscillators $(-)$ and for a finite amount of oscillators $(\cdots)$. The critical coupling strength is indicated with K_c [3].

N	**synchronization**	r	K	ω	**oscillators**
finite	partial synchronization	$0 < r < 1$	$0 < K < K_c$	$\lvert\omega\rvert > Kr$	independent
				$\lvert\omega\rvert < Kr$	locked
infinite	incoherent solution	$r = 0$	$K < K_c$	$\lvert\omega\rvert > Kr$	independent
	partial synchronization	$0 < r < 1$	$K_c < K < \infty$	$\lvert\omega\rvert > Kr$	independent
				$\lvert\omega\rvert < Kr$	locked
	global synchronization	$r = 1$	$K \to \infty$	$\lvert\omega\rvert < Kr$	locked

Table 1: Overview of the different domains for systems of coupled oscillators. N is the amount of oscillators, r the measure of phase coherence (defined as $|R|$ in equation (2.2)) and K the coupling parameter. The amount of synchronization is reflected in r. The natural frequency of the oscillators ω determines its behaviour on the long term. If an oscillator satisfies the inequality of the fifth column, its behaviour is described in the sixth column.

The stability of any of the solutions cannot be proven that easily. Linear stability analysis [3] has to be done in order to find out which solutions are stable [8, 29]. It can be shown that the

[3]A stationary or quasi-stationary solution to a non-linear system of differential equations is linearly unstable if the linearisation of the equation has eigenvalues with positive real part.[7]

incoherent state is linearly (neutrally) stable for $|K| < K_c$ and unstable otherwise. The trivial incoherent solution is neutrally stable [8]. For the phase-locked state, all but two eigenvalues are negative and merge into a continuous spectrum as the number of oscillators tends to infinity. One eigenvalue is always zero, by rotational invariance. The final eigenvalue, corresponding to a collective mode, determines the stability of the locked state [29]. *Chiba and Medvedev* [8] or *Mirollo and Strogatz* [29] can be read for more on stability.

3 Theory on Quantum Mechanics

3.1 Coherent States

In this section, the quantum mechanical theory needed to understand the derivations and conclusions of *Witthaut et al.* [1] is illustrated. To begin with, the quantization of the electromagnetic field is described in Section 3.1.1. This is the origin of the quantum mechanical field operators, which form the basis of the Heisenberg picture of quantum mechanics. In this representation, the operators (e.g. the observables) are time-dependent and the state-vectors are time independent. This is in contrast to the Schrödinger picture, in which the operators are constant and the quantum state is time-dependent. Throughout this thesis, the Heisenberg picture is used to describe the system. In this representation, the annihilation and creation operators represent the most prominent role of time-dependent operators. These non-observable operators will be introduced in Section 3.1.2. After the Fock number states and the quadrature operators are introduced in Sections 3.1.3 and 3.1.4, the coherent states can be defined and characterized. These are the states that will describe the quantum many-body system in *Witthaut et al.* [1] [4]. Therefore, this quantum background is needed to understand spin squeezing and number entanglement, and thus to derive the Kuramoto model for many-body entanglement.

3.1.1 Quantization of the Electromagnetic Field

The single-mode electromagnetic field can be expressed quantum mechanically. This is done by writing the classical expressions for both the electric and the magnetic field in terms of the corresponding quantum mechanical operators. The derivation is shortly explained here and is analogous to various books on quantum optics, for example *Introductory Quantum Optics* [17].

When the Maxwell equations are solved for a single-mode field, this results in the following expression for the electromagnetic field. The boundary conditions are taken such that the EM-waves are confined to a domain between two perfectly conducting walls. Therefore, the perturbation at both $z = 0$ and $z = L$ is zero for the electric field. The electric field is assumed to be polarized in the $\hat{x}$ direction, and thus the magnetic field in the $\hat{y}$ direction, as these are always orthogonal to each other and to the direction of propagation. The solutions of the Maxwell equations under these conditions are the following.

$$E_x(z,t) = \left(\frac{2\omega^2}{V\epsilon_0}\right)^{1/2} q(t)\sin(kz) \tag{3.2}$$

$$B_y(z,t) = \frac{\mu_0\epsilon_0}{k}\left(\frac{2\omega^2}{V\epsilon_0}\right)^{1/2} \dot{q}(t)\cos(kz) \tag{3.3}$$

In these equations, ω is the mode frequency and $k = \omega/c$ is the wave number. The time-dependent variable q represents the canonical position and therefore its derivative $\dot{q}$ stands for the canonical

[4] The actual states that are used in *Witthaut et al.* are two-mode spin coherent states. These are maximally localized in phase space and thus provide a natural link to the classical mean field dynamics of for example the Kuramoto model. Their definition is as follows [1]

$$|z,\Delta\phi\rangle = \frac{1}{\sqrt{N!}}\left(\sqrt{\frac{1+z}{2}}\hat{a}_1^\dagger + \sqrt{\frac{1-z}{2}}e^{-i\Delta\phi}\hat{a}_2^\dagger\right)^N |0\rangle \tag{3.1}$$

In this equation, $\hat{a}_1^\dagger$ is the creation operator for the first mode, and $\hat{a}_2^\dagger$ for the second. The parameters z and $\Delta\phi$ stand for the number difference and the phase difference between the two modes. The number difference gives a feeling for the difference in occupancy between the two modes. N is the total number of photons.

momentum of a unit mass. When the classical variables for the position and momentum are replaced with their quantum mechanical operators, the quantum mechanical expression for the electric and magnetic fields of a single mode is found.

$$\hat{E}_x(z,t) = \left(\frac{2\omega^2}{V\epsilon_0}\right)^{1/2} \hat{q}(t)\sin(kz) \tag{3.4}$$

$$\hat{B}_y(z,t) = \frac{\mu_0\epsilon_0}{k}\left(\frac{2\omega^2}{V\epsilon_0}\right)^{1/2} \hat{p}(t)\cos(kz) \tag{3.5}$$

The quantum mechanical operators must satisfy the canonical commutation relation

$$[\hat{q},\hat{p}] = i\hbar \tag{3.6}$$

The classical field energy of the single-mode field is given by the following Hamiltonian.

$$H = \frac{1}{2}\int \left(\epsilon_0 E_x^2(x,t) + \frac{1}{\mu_0}B_y^2(z,t)\right)dV \tag{3.7}$$

$$= \frac{1}{2}(p^2 + \omega^2 q^2) \tag{3.8}$$

It can be shown that these representations are equivalent, and thus the classical field energy of the electromagnetic wave is equivalent to the Hamiltonian of a harmonic oscillator of unit mass [17]. When this Hamiltonian is rewritten in quantum mechanical representation, this results the following Hamiltonian $\hat{H}$.

$$\hat{H} = \frac{1}{2}(\hat{p}^2 + \omega^2\hat{q}^2) \tag{3.9}$$

3.1.2 Creation and Annihilation Operators

In this light, the annihilation ($\hat{a}$) and creation ($\hat{a}^\dagger$) operators can be introduced. These operators are non-Hermitian, and therefore non-observable. They can be defined in terms of $\hat{q}$ and $\hat{p}$ as

$$\hat{a} = \frac{1}{\sqrt{2\hbar\omega}}(\omega\hat{q} + i\hat{p}) \tag{3.10}$$

$$\hat{a}^\dagger = \frac{1}{\sqrt{2\hbar\omega}}(\omega\hat{q} - i\hat{p}) \tag{3.11}$$

These are time-dependent operators, because the position and momentum operators are also time-dependent. Intuitively, the annihilation operator decreases and the creation operator increases the number of particles in a given state by one. This can be seen in equations (3.26) and (3.27) after the Fock number states are introduced in Section 3.1.3.

The annihilation and creation operator satisfy the commutation relation

$$[\hat{a},\hat{a}^\dagger] = 1 \tag{3.12}$$

With the annihilation and creation operator, the single-mode electromagnetic field operators (3.4) and (3.5) can be rewritten in the following way.

$$\hat{E}_x(z,t) = \mathcal{E}_0(\hat{a} + \hat{a}^\dagger)\sin(kz) \tag{3.13}$$

$$\hat{B}_y(z,t) = \frac{\mathcal{B}_0}{i}(\hat{a} - \hat{a}^\dagger)\cos(kz) \tag{3.14}$$

In these equations, $\mathcal{E}_0 = (\hbar\omega/\epsilon_0 V)^{1/2}$ and $\mathcal{B}_0 = (\mu_0/k)(\epsilon_0\hbar\omega^3/V)^{1/2}$ represent the electric and magnetic fields 'per photon' respectively. Note that the time dependence of both fields is included in the annihilation and creation operators.
The Hamiltonian operator (3.9) can now be written in the following form

$$\hat{H} = \hbar\omega\big(\hat{a}^\dagger\hat{a} + \frac{1}{2}\big) \tag{3.15}$$

This Hamiltonian can be used to determine time dependency of the newly introduced operators $\hat{a}$ and $\hat{a}^\dagger$, by substituting them in the Heisenberg equation of motion (3.16). When this is written out this results in the following differential equation, where the commutation relation as in equation (3.12) is used.

$$\begin{aligned}\frac{d\hat{a}}{dt} &= \frac{i}{\hbar}[\hat{H}, \hat{a}] && (3.16)\\ &= i\omega(\hat{a}^\dagger\hat{a}\hat{a} - \hat{a}\hat{a}^\dagger\hat{a}) \\ &= i\omega[\hat{a}^\dagger, \hat{a}]\hat{a} \\ &= -i\omega[\hat{a}, \hat{a}^\dagger]\hat{a} \\ &= -i\omega\hat{a} && (3.17)\end{aligned}$$

Which has the following exponential solution

$$\hat{a}(t) = \hat{a}(0)e^{-i\omega t} \tag{3.18}$$

In a similar way, the result that follows for the creation operator is

$$\hat{a}^\dagger = \hat{a}^\dagger(0)e^{i\omega t} \tag{3.19}$$

3.1.3 Fock Number States

With the annihilation and creation operator, the number operator $\hat{n}$ can be defined as

$$\hat{n} = \hat{a}^\dagger\hat{a} \tag{3.20}$$

The commutation relations between the number operator and the previously introduced annihilation and creation operator can be calculated very straightforwardly, and result in

$$[\hat{n}, \hat{a}^\dagger] = \hat{a}^\dagger \tag{3.21}$$

$$[\hat{n}, \hat{a}] = -\hat{a} \tag{3.22}$$

Note that the Hamiltonian for the electric field as given in equation (3.15) includes this number operator. The eigenstates $|n\rangle$ of the number operator are called the Fock number states. These states obey the equation

$$\hat{n}\,|n\rangle = n\,|n\rangle \tag{3.23}$$

These number states can be thought of as the states for the various energy levels of a harmonic oscillator, as the earlier mentioned Hamiltonian (3.15) describes the energy of a harmonic oscillator with unit mass. Fock states have a well-defined number of photons and a well defined energy, because the operator expresses both observables. Clearly, the energy operator $\hat{H}$ and the number operator $\hat{n}$ commute. The eigenvalue n of the number operator is interpreted as the number of photons in the field-mode. Therefore, the expectation value of the number operator

represents the mean number of photons in the corresponding mode, $\langle n \rangle = \bar{n}$. The amount of energy in a system is related to this average number of photons; the more photons present, the higher the energy value. The energy of each Fock state can therefore be expressed by

$$E_n = \hbar\omega(n + \frac{1}{2}), \quad n = 0, 1, 2, ... \tag{3.24}$$

The state for $n = 0$ is the vacuum state, in which there are no photons present. This state $|0\rangle$ has a non-zero energy value, namely $E_0 = \frac{1}{2}\hbar\omega$, which is a result of the commutation relation between the creation and annihilation operators, equation (3.12). These operators do not commute as the commutation relation does not equal zero.

Next to their corresponding energy value, some more characteristics of the number states will be discussed. Firstly, number states are normalised; $\langle n|n\rangle = 1$. Furthermore, states of different number are orthogonal, thus $\langle n'|n\rangle = \delta_{nn'}$. Therefore, they form an orthonormal complete set, which spans the Hilbert space or Fock space [17].

$$\sum_{n=0}^{\infty} |n\rangle \langle n| = 1 \tag{3.25}$$

When we let the annihilation and creation operators work on the number states, they work as ladder operators. In other words, the energy states will increase or decrease with one unit of 'quantum energy' $\hbar\omega$. Therefore, the operator $\hat{a}^\dagger$ is called the creation operator, as it creates one unit of quantum energy. Similarly, the annihilation operator $\hat{a}$ annihilates or destroys one quantum of energy. The following relations show this, with the corresponding pre-factor. This pre-factor is derived from the fact that the number states must be normalized.

$$\hat{a}\,|n\rangle = \sqrt{n}\,|n-1\rangle \tag{3.26}$$

$$\hat{a}^\dagger\,|n\rangle = \sqrt{n+1}\,|n+1\rangle \tag{3.27}$$

From this, it can be seen that the number states can be generated from the ground state, or vacuum state, $|0\rangle$ by letting the creation annihilator work repeatedly.

$$|n\rangle = \frac{(\hat{a}^\dagger)^n}{\sqrt{n!}}\,|0\rangle \tag{3.28}$$

Because the number states are orthogonal, the only matrix elements of the annihilation and creation operators that do not vanish are the following.

$$\langle n-1|\,\hat{a}\,|n\rangle = \sqrt{n}\,\langle n-1|n-1\rangle = \sqrt{n} \tag{3.29}$$

$$\langle n+1|\,\hat{a}^\dagger\,|n\rangle = \sqrt{n+1}\,\langle n+1|n+1\rangle = \sqrt{n+1} \tag{3.30}$$

With the relations previously derived, the expectation value and the quantum fluctuations of a single-mode electric field can be determined. The expectation value of the electric field operator, as expressed in equation (3.13) can be determined for a number state $|n\rangle$ in the following way

$$\langle n|\,\hat{E}_x(z,t)\,|n\rangle = \mathcal{E}_0 \sin(kz)[\langle n|\,\hat{a}\,|n\rangle + \langle n|\,\hat{a}^\dagger\,|n\rangle] = 0 \tag{3.31}$$

This results in a zero mean field, because the number states that result when the annihilation and creation operator are worked out are orthogonal. Therefore, the number state is not a state of

well-defined electric field. However, the expectation of the square of the electric field is non-zero.

$$\begin{aligned}\langle n|\,\hat{E}_x^2(z,t)\,|n\rangle &= \mathcal{E}_0^2\sin^2(kz)\,\langle n|\,\hat{a}^{\dagger 2}+\hat{a}^2+\hat{a}^\dagger\hat{a}+\hat{a}\hat{a}^\dagger\,|n\rangle \\ &= \mathcal{E}_0^2\sin^2(kz)\,\langle n|\,\hat{a}^{\dagger 2}+\hat{a}^2+2\hat{a}^\dagger\hat{a}+1\,|n\rangle \\ &= 2\mathcal{E}_0^2\sin^2(kz)\big(n+\frac{1}{2}\big)\end{aligned} \tag{3.32}$$

As the square of the electric field contributes to the energy density, and the number states are well-defined energy states, it could have been expected that this value is non-zero. This means that the electric field is a fluctuating quantity with a mean value of zero. These fluctuations in the field are characterized by the variance of the electric field operator, thus

$$\Big\langle(\Delta\hat{E}_x(z,t))^2\Big\rangle = \Big\langle\hat{E}_x^2(z,t)\Big\rangle - \Big\langle\hat{E}_x(z,t)\Big\rangle^2 \tag{3.33}$$

Combining equations (3.31), (3.32) and (3.33) thus gives the variance of the electric field operator. The uncertainty in this field is expressed by the standard deviation ΔE_x, which is the square root of the variance. Finally, the uncertainty in the electric field thus results in

$$\Delta E_x = \sqrt{2}\mathcal{E}_0\sin(kz)\big(n+\frac{1}{2}\big)^{1/2} \tag{3.34}$$

Thus even for the vacuum state $|0\rangle$, the quantized radiation field fluctuations are present. The cause for these vacuum fluctuations are the same as the cause for the zero-point energy, namely that the creation and annihilation operator do not commute.

3.1.4 Quadrature Operators

There are two more operators which are important to introduce for a single-mode field, namely the quadrature operators. These operators are represented by $\hat{X}_1$ and $\hat{X}_2$ and are associated with field amplitudes of the electric field.

In equation (3.13), the single-mode electric field is defined in terms of the annihilation and creation operator. These are, however, still time-dependent operators. When this time-dependence is explicitly included in the expression, this results in the following

$$\hat{E}_x = \mathcal{E}_0(\hat{a}e^{-i\omega t}+\hat{a}^\dagger e^{i\omega t})\sin(kz) \tag{3.35}$$

In this equation, $\hat{a}(0)\equiv\hat{a}$ and $\hat{a}^\dagger(0)\equiv\hat{a}^\dagger$, which are now independent of time. The quadrature operators are defined in terms of these newly defined annihilation and creation operator.

$$\hat{X}_1 = \frac{1}{2}(\hat{a}+\hat{a}^\dagger) \tag{3.36}$$

$$\hat{X}_2 = \frac{1}{2i}(\hat{a}-\hat{a}^\dagger) \tag{3.37}$$

The electric field can now be rewritten in terms of these operators.

$$\hat{E}_x = 2\mathcal{E}_0\sin(kz)[\hat{X}_1\cos(\omega t)+\hat{X}_2\sin(\omega t)] \tag{3.38}$$

From this expression it is clear why the quadrature operators are associated with field amplitudes of the electric field. They oscillate out of phase by 90° and are hence in quadrature. They satisfy the following commutation relation

$$[\hat{X}_1,\hat{X}_2] = \frac{i}{2} \tag{3.39}$$

The uncertainty relation that follows is

$$\left\langle (\Delta \hat{X}_1)^2 \right\rangle \left\langle (\Delta \hat{X}_2)^2 \right\rangle \geq \frac{1}{16} \tag{3.40}$$

The expectation value of the quadrature operators for the number states is zero, $\langle n| \hat{X}_1 |n\rangle = \langle n| \hat{X}_2 |n\rangle = 0$. However, the second moment is non-zero and can be derived by

$$\begin{aligned} \langle n| \hat{X}_1^2 |n\rangle &= \frac{1}{2} \langle n| \hat{a}^2 + \hat{a}^{\dagger 2} + \hat{a}^\dagger \hat{a} + \hat{a}\hat{a}^\dagger |n\rangle \\ &= \frac{1}{4} \langle n| \hat{a}^2 + \hat{a}^{\dagger 2} + 2\hat{a}^\dagger \hat{a} + 1 |n\rangle \\ &= \frac{1}{4}(2n+1) \end{aligned} \tag{3.41}$$

The same derivation holds for $\hat{X}_2$, thus

$$\langle n| \hat{X}_2^2 |n\rangle = \frac{1}{4}(2n+1) \tag{3.42}$$

For a number state, the uncertainties are therefore the same for both quadratures. Particularly, for the vacuum state $|0\rangle$, the uncertainty product is minimized. The following relation holds.

$$\left\langle (\Delta \hat{X}_1)^2 \right\rangle_{\text{vac}} = \left\langle (\Delta \hat{X}_2)^2 \right\rangle_{\text{vac}} = \frac{1}{4} \tag{3.43}$$

The relations that represent the uncertainties in these quadrature operators will be used in Sections 3.1.6 and 3.2.1 to compare number states, coherent states and squeezed states. Figure 5 (Section 3.2) is the phase-space portrait of each of these states, and gives insight in their uncertainty characteristics.

3.1.5 Definition of Coherent States

Coherent states can be defined in two ways, which will be explained briefly. [5]

Firstly, coherent states are the eigenstates of the annihilation operator. These 'right' eigenstates $|\alpha\rangle$ satisfy the following relation, with eigenvalue α. This eigenvalue may be complex, as the annihilation operator is non-Hermitian.

$$\hat{a} |\alpha\rangle = \alpha |\alpha\rangle \tag{3.44}$$

For the creation operator, the states $\langle\alpha|$ are 'left' eigenstates with eigenvalue α^*.

$$\langle\alpha| \hat{a}^\dagger = \alpha^* \langle\alpha| \tag{3.45}$$

When these coherent states $|\alpha\rangle$ are expanded in terms of the number states $|n\rangle$ and the normalization requirement is met, the expression for these states is the following [17]

$$|\alpha\rangle = \exp\left(-\frac{1}{2}|\alpha|^2\right) \sum_{n=0}^{\infty} \frac{\alpha^n}{\sqrt{n!}} |n\rangle \tag{3.46}$$

[5] Coherent states can actually be defined in three ways. The third definition is based on the most important characteristic of coherent states, described in Section 3.1.6. Namely, that coherent states are states with a minimum-uncertainty relationship. However, this definition is not unique. For example, the ideal squeezed states as discussed in Section 3.2 also obey this definition as well as they also minimize the uncertainty [44]

Secondly, coherent states can be defined as displaced vacuum states. The Glauber displacement operator is defined as

$$\hat{D}(\alpha) = \exp\big(\alpha\hat{a}^\dagger - \alpha^*\hat{a}\big) \tag{3.47}$$

This operator is unitary, which means that

$$\hat{D}^\dagger(\alpha) = \hat{D}(-\alpha) = \big(\hat{D}(\alpha)\big)^{-1} \tag{3.48}$$

If this operator acts on a vacuum state $|0\rangle$, this results in a coherent state.

$$|\alpha\rangle = \hat{D}(\alpha)\,|0\rangle \tag{3.49}$$

Working this out results in the same definition as from the eigenstates of the annihilation operator, given in equation (3.46) [17].

3.1.6 Characteristics of Coherent States

The most important property of coherent states is that they are minimum uncertainty states. In other words, these are the states for which the Heisenberg uncertainty relation for two Hermitian operators is minimized [4].

When the three Hermitian operators $\hat{A}$, $\hat{B}$ and $\hat{C}$ satisfy the commutation relation (3.50), they satisfy the Heisenberg uncertainty relation (3.51) [17].

$$[\hat{A}, \hat{B}] = i\hat{C} \tag{3.50}$$

$$\langle(\Delta\hat{A})^2\rangle\langle(\Delta\hat{B})^2\rangle \geq \frac{1}{4}\langle(\Delta\hat{C})^2\rangle \tag{3.51}$$

For coherent states however, the uncertainty in operators $\hat{A}$ and $\hat{B}$ are minimized such that the equality in the uncertainty relation (3.51) holds. [6]

Additionally, coherent states always have the following Poisson photon number distribution. In other words, when measuring the number of photons in the field the probability of detecting n photons is described by the following probability distribution [4, 17]

$$P(n) = |\,\langle n|\alpha\rangle\,|^2 = \exp\big(-|\alpha|^2\big)\frac{|\alpha|^{2n}}{n!} \tag{3.52}$$

The mean of this distribution is $|\alpha|^2$, which is the expectation value of the photon number operator $\hat{n}$ in coherent state $|\alpha\rangle$.

$$\bar{n} = \langle n\rangle = \langle\alpha|\,\hat{n}\,|\alpha\rangle = \langle\alpha|\,\hat{a}^\dagger\hat{a}\,|\alpha\rangle = |\alpha|^2 \tag{3.53}$$

Therefore, the probability distribution (3.52) can be rewritten into

$$P(n) = \frac{\bar{n}^n e^{-\bar{n}}}{n!} \tag{3.54}$$

[6] Applying this minimum uncertainty relation to the position operator $\hat{q}$ and momentum operator $\hat{p}$ was the original motivation for Schrödinger to propose the coherent states. These states follow the classical motion of the harmonic oscillator [44].

which can clearly be recognised as a Poissonian distribution.

Where the number states are orthogonal, normalized and complete (see Section 3.1.2), the coherent states are normalized, but not orthogonal and overcomplete [17, 38].

The normalization follows from the definition directly. As the displacement operator is unitary, it follows with equation (3.48) that

$$\langle\alpha|\alpha\rangle = \langle 0|\,\hat{D}^\dagger(\alpha)\hat{D}(\alpha)\,|0\rangle = 1 \tag{3.55}$$

The coherent states are not orthogonal. This can be derived from the definition (3.46) for two coherent states $|\alpha\rangle$ and $|\beta\rangle$ [17].

$$|\,\langle\beta|\alpha\rangle\,|^2 = e^{-|\beta-\alpha|^2} \neq 0 \tag{3.56}$$

By integrating over the complex α-plane, completeness can be shown. This results in [17]

$$\int |\alpha\rangle\,\langle\alpha|\,\frac{d^2\alpha}{\pi} = 1 \tag{3.57}$$

However, the coherent states $|\alpha\rangle$ are overcomplete. That is, some eigenstates could be left out such that the system or set is still complete. This can be intuitively supported by the fact that the coherent states are not orthogonal; there could be a representation or integral which does not include all coherent states but does result in a unit answer [30, 38].

Coherent states are very close to classical states, mainly due to the minimum uncertainty relation that they obey. Due to this minimized uncertainty and therefore minimal fluctuations, coherent states are maximally localized in phase space. Phase space is the infinite (complex) plane of eigenvalues that belong with two Hermitian operators [14]. Phase space portraits are shown in Figure 5 (Section 3.2). The radius of the circle represents the uncertainty in the two operators or quadratures. Therefore, the coherent state has the smallest radius and is therefore maximally localized in phase space.

Moreover, a few more characteristics of coherent states will be discussed, which cause these states to resemble classical physics.

Firstly, coherent states have an expectation value of the electric field that is of the classical form, in contrast with those of the number states. Recall that the expectation of the electric field operator was zero for the number states, see equation (3.31). For coherent states however, this is not the case.

Additionally, the fluctuations in the fractional uncertainty for the photon number decrease with an increasing average photon number. Therefore, the states become well localized in phase with increasing average photon number, which makes them resemble classical states. To explore this mathematically, the fluctuation of photon number can be calculated. Recall that the first moment, the expectation value of the number operator $\hat{n}$, is equal to $|\alpha|^2$, see equation (3.53). The second moment is calculated by

$$\begin{aligned}\langle\alpha|\,\hat{n}^2\,|\alpha\rangle &= \langle\alpha|\,\hat{a}^\dagger\hat{a}\hat{a}^\dagger\hat{a}\,|\alpha\rangle \\ &= \langle\alpha|\,(\hat{a}^\dagger\hat{a}^\dagger\hat{a}\hat{a} + \hat{a}^\dagger\hat{a})\,|\alpha\rangle \\ &= |\alpha|^4 + |\alpha|^2 = \bar{n}^2 + \bar{n}\end{aligned} \tag{3.58}$$

Thus the fluctuations in photon number are

$$\Delta n = \sqrt{\langle \hat{n}^2 \rangle - \langle \hat{n} \rangle^2} = \sqrt{\bar{n}} = |\alpha| \tag{3.59}$$

This is again characteristic for a Poissonian process thus in accordance with the probability distribution (3.54). The fractional uncertainty in the photon number is given by

$$\frac{\Delta n}{\bar{n}} = \frac{1}{\sqrt{\bar{n}}} = \frac{1}{|\alpha|} \tag{3.60}$$

Note this uncertainty decreases with an increasing average number of photons, and thus an increasing field strength.

3.1.7 Standard Quantum Limit

In this light, the Standard Quantum Limit can be examined shortly. This shot noise limit is the limit that refers to the minimum level of quantum noise which is obtainable without squeezed states (Section 3.2), given by

$$\Delta\varphi \geq \frac{1}{\sqrt{N}} \tag{3.61}$$

For coherent states, the quantum fluctuations are minimal, and thus equal to $\frac{1}{\sqrt{N}}$. This is valid for all N-photon separable states, thus in the absence of entanglement between the photons [11, 21, 24].

Inequality (3.61) shows the uncertainty in the photon number given by equation (3.59) is the minimal value that it could have. Therefore, in coherent states the uncertainty in the number of photons in a certain state is indeed minimized. This holds for all observables, which is why coherent states are called minimal uncertainty states [4, 17].

3.2 Squeezed States

We saw in Section 3.1.6 that when the three Hermitian operators $\hat{A}$, $\hat{B}$ and $\hat{C}$ satisfy the commutation relation $[\hat{A}, \hat{B}] = i\hat{C}$, they satisfy the Heisenberg uncertainty relation

$$\langle(\Delta\hat{A})^2\rangle\langle(\Delta\hat{B})^2\rangle \geq \frac{1}{4}\langle(\Delta\hat{C})^2\rangle \tag{3.62}$$

A state of the system is a squeezed state if either [17, 31]

$$\left\langle(\Delta\hat{A})^2\right\rangle < \frac{1}{2}\left|\left\langle\hat{C}\right\rangle\right| \qquad \text{or} \qquad \left\langle(\Delta\hat{B})^2\right\rangle < \frac{1}{2}\left|\left\langle\hat{C}\right\rangle\right| \tag{3.63}$$

Intuitively, this means that the uncertainty in one of the operators is diminished, therefore the fluctuations are smaller. The other operator however will have a larger uncertainty, because the Heisenberg equation (3.62) must be satisfied.

Ideal sqeezed states can be defined as sqeezed states for which the equality in the Heisenberg uncertainty relation (3.62) holds. The product of the two uncertainties is therefore as small as possible, thus the variances satisfy the minimum-uncertainty relation. These ideal squeezed states can be obtained from the coherent states with a scale transformation that compresses one axis and dilates the other. Visually, in a phase-space plot, the circle that represents a coherent state is transformed into an ellipse; one direction is stretched out whereas the other is pushed in. This is visualised in Figure 5 [10, 31].

Figure 5 shows the phase space plots of various states on the left, and a plot of the electric field in time on the right [31]. The classical expression for the electric field would be a sine without any uncertainty or fluctuations.

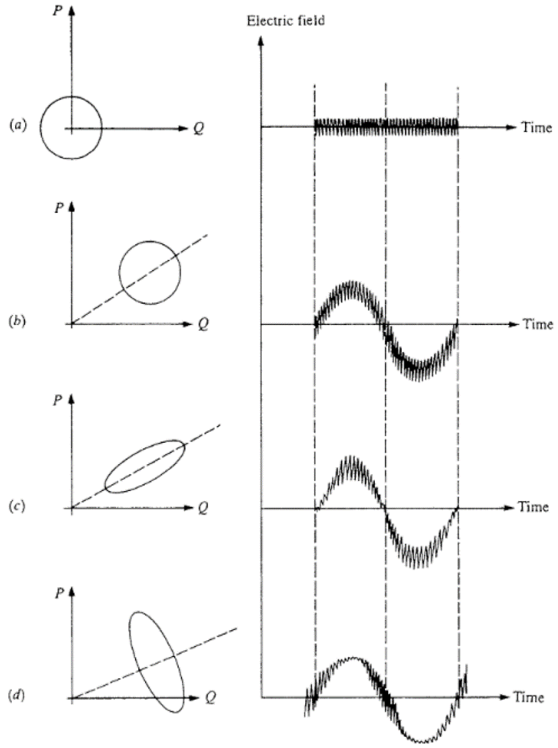

Figure 5: The left column shows phase-space plots of various states and the right column shows the corresponding plot of the electric field in time. The visualised states are: (a) vacuum state, (b) coherent state, (c) squeezed state with reduced phase uncertainty (d) squeezed state with reduced amplitude uncertainty [31].

The radius of the phase-space plots represent the uncertainty in the of the state. When one would compare the coherent or vacuum states with the Fock number states, the number states would thus have a larger radius.

3.2.1 Quadrature Squeezing

When the operators in equations (3.63) are taken to be the quadrature operators, $\hat{A} = \hat{X}_1$ and $\hat{B} = \hat{X}_2$, it follows from equation (3.40) that $\hat{C} = \frac{1}{2}$. Consequently, quadrature squeezing occurs whenever

$$\left\langle (\Delta \hat{X}_1)^2 \right\rangle < \frac{1}{4} \qquad \text{or} \qquad \left\langle (\Delta \hat{X}_2)^2 \right\rangle < \frac{1}{4} \tag{3.64}$$

For both the vacuum state and the coherent state, both quadratures had an uncertainty of $\frac{1}{4}$. Therefore, a quadrature squeezed state is present when the uncertainty in one of the quadrature operators is less than the uncertainty of the vacuum state $|0\rangle$ or the coherent state $|\alpha\rangle$. One of the quadratures has less noise, thus the fluctuations in this quadrature are said to be squeezed. As a consequence, the fluctuations in the other quadrature are larger than those of $|0\rangle$ or $|\alpha\rangle$, since the Heisenberg uncertainty relation must always hold.

After discussing the properties of these squeezed states, it is important to note how to generate a squeezed state mathematically. In order to do so, the squeeze operator $\hat{S}(\xi)$ is defined

as

$$\hat{S}(\xi) = \exp\left(\frac{1}{2}(\xi^* \hat{a}^2 - \xi \hat{a}^{\dagger 2})\right) \tag{3.65}$$

In this definition, $\xi = re^{i\theta}$. Parameter r is known as the squeeze parameter and takes values between $0 \leq r < \infty$. Parameter θ takes values between $0 \leq \theta \leq 2\pi$. When the squeezing operator acts on the vacuum state $|0\rangle$, the wave function of the squeezed vacuum is obtained.

$$|0, \xi\rangle = \hat{S}(\xi)\,|0\rangle \tag{3.66}$$

This is an ideal squeezed state, and the method for deriving the squeezing operator boils down to the scale transformation as introduced in Section 3.2.1. The parameter $\xi = re^{i\theta}$ shows that the transformation is a combination of squeezing and rotation. The amount of squeezing is thus represented by the squeeze parameter r, as might be expected. The angle under which the squeezing is applied is $\frac{\theta}{2}$. The squeezing operator corresponds to a compression in the quadrature at $\frac{\theta}{2}$ and a dilation in the quadrature at $\frac{\theta}{2} + \frac{\pi}{2}$ [10].

More generally, the family of ideal squeezed states is generated by displacing the squeezed vacuum with the displacement operator $\hat{D}(\alpha)$ as introduced previously in Section 3.1.5.

$$|\alpha, \xi\rangle = \hat{D}(\alpha)\hat{S}(\xi)\,|0\rangle \tag{3.67}$$

The same resulting minimum-uncertainty state can be obtained by applying the squeezing operator to a coherent state. The squeezing operator and the displacement operator do however not commute, but the same state can be obtained with a different parameter α [17].

The average number of photons in a squeezed state can be obtained by determining the expectation value of the number operator.

$$\langle \alpha, \xi |\, \hat{n}\, | \alpha, \xi \rangle = |\alpha|^2 + \sinh^2(r) \tag{3.68}$$

When one looks at the number of photons in a squeezed vacuum, where $|\alpha|^2 = 0$, the above expression however does not go to zero. The fact that the average number of photons in the squeezed vacuum state is non-zero shows that energy is required to squeeze the vacuum [10].

3.2.2 Spin Squeezing

Spin squeezing aims to redistribute the fluctuations of two conjugate spin directions among each other. Spin squeezing can indicate an entangled state, and is therefore used to detect the presence of entanglement [1, 21]. The name 'spin squeezing' does not originate from the fact that the physical spin would in a way be squeezed, but because N particles can be described by a fictitious spin $J = \frac{N}{2}$ [16]. In this section, the mathematical concept of spin squeezing will be introduced. When this concept is known, entanglement criteria can be defined in Section 3.3.

We consider one two-mode system or atom with modes $|1\rangle$ and $|2\rangle$. This can be mapped onto a spin $J = \frac{1}{2}$ system. Any observable with a spin J system can be expressed by the three spin operators $\hat{J}_x$, $\hat{J}_y$, $\hat{J}_z$ and the identity operator. This simplest system is described in the following way.

State $|1\rangle$ is mapped to the eigenstate of $\hat{J}_z$ with eigenvalue $-\frac{1}{2}$ (spin down) and state $|2\rangle$ is mapped to the eigenstate with eigenvalue $+\frac{1}{2}$ (spin up). Any pure quantum state of a two-level system described by

$$|\theta, \phi\rangle = \sin(\theta/2)\,|1\rangle + \cos(\theta/2)e^{i\phi}\,|2\rangle \tag{3.69}$$

can now be depicted on a Bloch sphere, as shown in Figure 6 [16, 21].

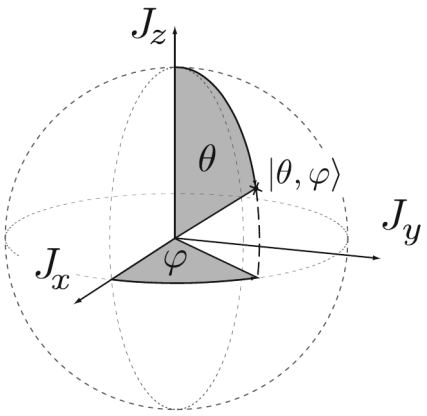

Figure 6: Schematic representation of the quantum state $|\theta, \phi\rangle$ of a spin-$\frac{1}{2}$ system on a Bloch Sphere [21].

This description of a single system or atom consisting of two modes can be generalized for N particles, where each particle is restricted to two modes. There are no quantum correlations present between the particles. The collective spin is defined as the sum over all elementary spin operators, or Pauli matrices. [7] The derivation of this total spin system can be read in *Groß* [21]. The expression for the total state $|\theta, \varphi\rangle$ is the following.

$$|\theta, \varphi\rangle = \frac{1}{\sqrt{N!}} \left(\sin(\theta/2)\hat{a}_1^\dagger + \cos(\theta/2)\exp(i\varphi)\hat{a}_2^\dagger \right)^N |0\rangle \tag{3.70}$$

Therefore, the generalized Bloch sphere now describes the mean spin direction and its fluctuations.

The earlier mentioned operators which can describe the spin-$\frac{1}{2}$ system are defined below for the generalization to N particles. Squeezing can be quantified using these fictitious spin components [1, 16, 21].

$$\hat{J}_z = \frac{1}{2}(\hat{a}_2^\dagger \hat{a}_2 - \hat{a}_1^\dagger \hat{a}_1) \tag{3.71}$$

$$\hat{J}_y = \frac{i}{2}(\hat{a}_2^\dagger \hat{a}_1 - \hat{a}_1^\dagger \hat{a}_2) \tag{3.72}$$

$$\hat{J}_x = \frac{1}{2}(\hat{a}_2^\dagger \hat{a}_1 + \hat{a}_1^\dagger \hat{a}_2) \tag{3.73}$$

These operators together form an angular momentum algebra [1]. Note that the operator $\hat{J}_z$ actually represents half the atom number difference between the modes. Namely, it can be rewritten as $\hat{J}_z = \frac{1}{2}(\hat{n}_2 - \hat{n}_1)$, with the number operators as defined in Section 3.1.3.

The three orthogonal spin components are conjugate variables. The commutation relation

[7] The definition in terms of Pauli matrices will be used in Section 3.3.2, equations (3.71) to (3.73).

between these operators is described in equation (3.75), with ϵ_{ijk} the Levi-Civita symbol [21]. [8]

$$[\hat{J}_i, \hat{J}_j] = i\epsilon_{ijk}\hat{J}_k \tag{3.75}$$

Consequently, any pair of spin operators obeys a Heisenberg uncertainty relation. For example, for $\hat{J}_z$ and $\hat{J}_y$ this is [21, 34]

$$(\Delta\hat{J}_z)^2(\Delta\hat{J}_y)^2 \geq \frac{1}{4}(\Delta\hat{J}_x)^2 \tag{3.76}$$

The variance in each direction is given by $\Delta\hat{J}_x = \langle\hat{J}_x^2\rangle - \langle\hat{J}_x\rangle^2$. For the operator $\hat{J}_x$, the expectation value is however equal to zero. Therefore, the only resulting term is $\frac{1}{4}\langle\hat{J}_x^2\rangle = \frac{J}{4}$. This gives

$$(\Delta\hat{J}_z)^2(\Delta\hat{J}_y)^2 \geq \frac{J}{4} \tag{3.77}$$

In this equation, J is the total spin length, for which $J = \frac{N}{2}$ [21]. For a coherent spin state, this uncertainty relation again reduces to the equality due to their minimum uncertainty characteristics. When no quantum correlations between the particles are present, which is the case for coherent states, the variance in each direction $\hat{J}_\perp$ orthogonal to the mean spin direction (θ, ϕ) are equal.

$$\Delta\hat{J}_z^2 = \Delta\hat{J}_y^2 = \frac{J}{2} \tag{3.78}$$

Recall the standard quantum limit (3.61) discussed in Section 3.1.7. The variable $\Delta\varphi$ can be seen as the isotropic angular uncertainty; the uncertainty of the perpendicular spin directions $\Delta\hat{J}_\perp$ to the mean spin length J [21]. The derivation of this limit for coherent state fluctuations is relatively easy when considering the spin representation.

$$\Delta\varphi = \frac{\Delta\hat{J}_\perp}{\langle\hat{J}\rangle} = \frac{1}{\sqrt{2J}} = \frac{1}{\sqrt{N}} \tag{3.79}$$

Spin squeezing or number squeezing

Now that we know how N particles can be described by a fictitious spin J, the spin squeezed states can be defined. Quantum states are considered to be spin squeezed if the variance of one spin component is smaller than the shot noise limit for a coherent spin state, which is $\frac{J}{2}$ as in equation (3.78). Note that this definition is completely analogous to the definition of squeezed states in general (3.63), but is now applied to the spin operators that describe the system. Due to the Heisenberg uncertainty relation, the variance in the other direction will increase [1, 16, 21, 32, 34].

Coherent spin squeezing can also be referred to as coherent number squeezing, because the purely theoretical spin has links to the number of atoms occupying a certain state. Remember that the operator $\hat{J}_z$ represents half the atom number difference. When a system is spin-squeezed in the $\hat{J}_z$ direction, this is equivalent to

$$(\Delta\hat{J}_z)^2 < \frac{J}{2} \tag{3.80}$$

[8] The Levi-Civita symbol is a discrete function of three variables, defined in the following way.

$$\epsilon_{ijk} = \begin{cases} +1 & \text{if } (i,j,k) \text{ is (1,2,3), (2,3,1) or (3,1,2)} \\ -1 & \text{if } (i,j,k) \text{ is (3,2,1), (1,3,2) or (2,1,3)} \\ 0 & \text{if } i=j,\ j=k \text{ or } k=i \end{cases} \tag{3.74}$$

In other words, the atom number fluctuations are squeezed or diminished. In practice, this boils down to two observations. First, the mean angular momentum of the state is large. Secondly, the variance of the angular momentum in a direction orthogonal to the mean direction is small. This number squeezing can be used to detect entanglement and to enable high precision metrology, which will be discussed in Section 3.3. [1, 16, 21, 32]

Spin squeezing was one of the first ways found to overcome the standard quantum limit (*Wineland et al.* [39]). This is valuable, as quantum research often requires very precise measurements. Spin squeezing is therefore applied in (non-linear) quantum optics and interferometry [43, 21]. However, it was found in 2001 that spin squeezing can also be applied to achieve entanglement in Bose-Einstein condensates, which can thereafter be used for information processing [16, 32].

3.3 Number Entanglement

Coherent spin squeezing, or coherent number squeezing, amongst N particles is related to many-body entanglement. In this section, many-body entanglement will be defined. After this, we can see how spin squeezing indicates many-body entanglement. This will be done by introducing a criterion for the squeezing parameter ξ^2, which can be defined with the variables discussed in Section 3.2.2.

3.3.1 Many-Body Entanglement

Entanglement in many-body systems is defined as the non-separability of the density matrix.

The Density Matrix
The density matrix or density operator $\hat{\rho}$ is an alternate representation of the quantum state, which is equivalent to description with a wave function $|\psi\rangle$. The formal definition for this density operator is the following

$$\hat{\rho} = |\psi\rangle \langle\psi| = \sum_i p_i |\psi_i\rangle \langle\psi_i| \tag{3.81}$$

In this definition, p_i is the probability of the system being in the ith state $|\psi_i\rangle$ [17].

The density operator has a few important characteristics, which will not be derived here. [9] These properties are:

1. $\hat{\rho}$ is Hermitian
2. $\mathrm{Tr}\,\hat{\rho} = 1$ [10]
3. $\mathrm{Tr}\,\hat{\rho}^2 \begin{cases} = 1 & \text{for a pure state} \\ < 1 & \text{for a mixed state} \end{cases}$
4. $\langle\hat{A}\rangle = \mathrm{Tr}\left(\hat{\rho}\hat{A}\right)$

In the third property, pure and mixed states are distinguished. A pure quantum state can be described by state vectors only, mixed states cannot as they are a probabilistic mixture of pure states. Therefore, the density operator reduces to $\hat{\rho} = |\psi_j\rangle \langle\psi_j|$ for pure states because all other probabilities p_i for $i \neq j$ vanish and $p_j = 1$ [17, 31].

When the N-particle density matrix $\hat{\rho}$ is inseparable, the quantum state is known to be entangled. A matrix is separable if it can be decomposed in the following way [17, 32]

$$\hat{\rho} = \sum_i p_i \; \hat{\rho}_i{}^{(1)} \otimes \hat{\rho}_i{}^{(2)} \otimes ... \otimes \hat{\rho}_i{}^{(N)} \tag{3.82}$$

with p_i the probability for state i and $\hat{\rho}_i^{(k)}$ a density matrix for the kth particle. For non-entangled systems, the total density matrix can thus be decomposed into density matrices for each particle by itself. This intuitively corresponds with the definition of entangled particles; those who interact in ways such that the state of each particle can not be described independently. An entangled quantum system must be described as a whole and therefore the density matrix cannot be split up. [1, 16, 18, 32]

[9] For more background information, one can read *Gerry and Knight* [17] or *Scully and Zubairy* [31].

[10] Tr means taking the trace of the matrix; summation of the diagonal matrix elements. This second property thus expresses the normalization of any state described by the density matrix.

3.3.2 Entanglement Criterion

The earlier discussed spin squeezing (Section 3.2.2) and many-body entanglement (Section 3.3.1) are linked. In Bose-Einstein condensates, spin squeezing is one of the most successful approaches for creating many-body entanglement [16, 18, 32]. [11] Furthermore, spin squeezing can be used to show the presence of entanglement. This property is most important for understanding the main research of *Witthaut et al.* [1]. In order to show that the Kuramoto model can be used to describe entanglement in Bose-Einstein condensates, one must be able to detect when entanglement is present.

More generally, when quantum experiments require entanglement, it is important to detect it as well. The creation of an entangled state is often followed by measurements to make sure that the produced state was indeed entangled. In many-particle experiments however, it is often impossible to address the particles individually [34]. Therefore, it is important to derive conditions such that it is possible to create and detect entanglement with collective operations. In most many-particle experiments, observables are limited to the first and second order moments of the distribution functions in different spin directions [21]. This is mainly due to small counting statistics and technical noise [21]. Therefore, it would be suitable if these moments could be used to derive a criterion for many-particle entanglement.

As stated in *Estève et al.* [16] "The fluctuation measurement of the two conjugate variables, number and phase, yields information about the quantum state of the system and, in particular, allows for the detection of macroscopic entanglement between the particles." It can be shown that when one is able to detect number squeezing (spin-squeezing in the $\hat{J}_x$ direction), this implies the presence of entanglement immediately. This implication of number squeezing to entanglement will be discussed by introducing the squeezing parameter ξ^2 and its entanglement criterion, as used in *Witthaut et al* [1]. This is only one of the criteria which can be used to detect entanglement, though it is the most commonly used. There are more inequalities which imply the violation of the separability of the density operator, which can be found in for example [18, 21].

With the parameters and operators introduced in Section 3.2.2 to describe N particles with two modes as a spin J system, a squeezing parameter ξ^2 can be defined.

$$\xi^2 = N\frac{\Delta\hat{J}_z^2}{\langle\hat{J}_x\rangle^2 + \langle\hat{J}_y\rangle^2} \tag{3.83}$$

For separable states, the squeezing parameter obeys $\xi^2 \geq 1$. For entangled states however, the squeezing parameter will decline to a value $\xi^2 < 1$. The entanglement properties of the system can be expressed in terms of the spin operators, such that the spin squeezed states for which the entanglement parameter is smaller than one will always be entangled [1, 16, 18, 21, 32].

The proof for the easiest example of a two particle system with pure states will be given first. Assume that the particles are non-entangled, their density matrix is separable. The squeezing parameter will be shown to have a value larger or equal to one.

Note that the definitions of the spin component operators (equations (3.71) to (3.73)) can be

[11] Bose-Einstein condensates are particularly useful for entanglement theory, because they can be considered pure at single particle level. This is a crucial requirement for the production of entangled states. A method to achieve this is by applying a resonant laser pulse to all atoms in the condensate. These atoms are then allowed to evolve freely, so that collisional interactions produce entanglement between the atoms [32]

rewritten in terms of the Pauli matrices, as the collective spin was defined as the sum over all elementary Pauli matrices (footnote 7 page 27). For two particles, this reduces to the following definitions [21, 32].

$$\hat{J}_z = \frac{1}{2}\big(\sigma_z^{(1)} + \sigma_z^{(2)}\big) \tag{3.84}$$

$$\hat{J}_y = \frac{1}{2}\big(\sigma_y^{(1)} + \sigma_y^{(2)}\big) \tag{3.85}$$

$$\hat{J}_x = \frac{1}{2}\big(\sigma_x^{(1)} + \sigma_x^{(2)}\big) \tag{3.86}$$

In these equations, the usual definition of the Pauli matrices holds. [12] The upper index $^{(1)}$ or $^{(2)}$ indicates which particle the operator works upon.

To determine ξ^2, the values for $\Delta\hat{J}_z{}^2 = \langle\hat{J}_z{}^2\rangle - \langle\hat{J}_z\rangle^2$, $\langle\hat{J}_x\rangle^2$ and $\langle\hat{J}_y\rangle^2$ have to be determined. From the definition (3.84)

$$\hat{J}_z{}^2 = \frac{1}{4}\bigg((\sigma_z^{(1)})^2 + (\sigma_z^{(2)})^2 + 2\sigma_z^{(1)}\sigma_z^{(2)}\bigg) = \frac{1}{2}\big(I + \sigma_z^{(1)}\sigma_z^{(2)}\big) \tag{3.88}$$

This gives an expectation value of

$$\langle\hat{J}_z{}^2\rangle = \frac{1}{2}\big(1 + \langle\sigma_z^{(1)}\rangle\langle\sigma_z^{(2)}\rangle\big) \tag{3.89}$$

However, this expectation value is the same for both particles. [13] Therefore

$$\langle\hat{J}_z{}^2\rangle = \frac{1}{2}\big(1 + \langle\sigma_z\rangle^2\big) \tag{3.90}$$

Similarly, in the expression for $\langle\hat{J}_z\rangle^2$, the four terms that occur when expanding the brackets are all equal.

$$\langle\hat{J}_z\rangle^2 = \frac{1}{4}\bigg(\langle\sigma_z^{(1)}\rangle + \langle\sigma_z^{(2)}\rangle\bigg)^2 = \langle\sigma_z\rangle^2 \tag{3.91}$$

The same can be written for spin directions x and y, thus

$$\langle\hat{J}_x\rangle^2 = \langle\sigma_x\rangle^2 \tag{3.92}$$

$$\langle\hat{J}_y\rangle^2 = \langle\sigma_y\rangle^2 \tag{3.93}$$

The variance in spin z can be found from expressions (3.90) and (3.91)

$$(\Delta\hat{J}_z)^2 = \frac{1}{2}\big(1 - \langle\sigma_z\rangle^2\big) \tag{3.94}$$

With these calculations, the squeezing parameter is reduced to the expression below. The factor $\frac{1}{2}$ in the variance cancels to the factor $N = 2$, resulting in

$$\xi^2 = \frac{1 - \langle\sigma_z\rangle^2}{\langle\sigma_x\rangle^2 + \langle\sigma_y\rangle^2} \tag{3.95}$$

[12] The Pauli matrices are defined in the following way.

$$\sigma_z = \begin{pmatrix} 1 & 0 \\ 0 & -1 \end{pmatrix} \qquad \sigma_y = \begin{pmatrix} 0 & -i \\ i & 0 \end{pmatrix} \qquad \sigma_x = \begin{pmatrix} 0 & 1 \\ 1 & 0 \end{pmatrix} \tag{3.87}$$

[13] We assume that the two particles are identical, thus $|\psi\rangle = |\psi^{(1)}\rangle \otimes |\psi^{(1)}\rangle$.

Now assume that the quantum state which the squeezing parameter is determined for is pure. To simplify, we can write this state as the simple vector

$$|\Psi\rangle = \begin{pmatrix} a \\ b \end{pmatrix} \tag{3.96}$$

In this vector a and b might be complex valued and the vector must be normalized. This notation might seem like a simplification, but may be used as each pure state can be described by a vector in Hilbert space. In fact, only the normalization of this vector is what will be needed to prove the inequality for the squeezing parameter ξ^2. With this state, the expectation values result in

$$\langle\Psi|\,\sigma_z\,|\Psi\rangle^2 = |a|^4 + |b|^4 - 2|ab|^2 \tag{3.97}$$

$$\langle\Psi|\,\sigma_x\,|\Psi\rangle^2 = (a^*b)^2 + (b^*a)^2 + 2|ab|^2 \tag{3.98}$$

$$\langle\Psi|\,\sigma_y\,|\Psi\rangle^2 = -(a^*b)^2 - (b^*a)^2 + 2|ab|^2 \tag{3.99}$$

Substituting this into equation (3.95) and using the normalization of $|\Psi\rangle$ gives $\xi^2 = 1$. Therefore, this separable (thus non-entangled) state obeys the inequality $\xi^2 \geq 1$.

Now for a mixed two particle quantum state, the state cannot be written as a vector of Hilbert space. The density matrix is needed to determine the value of ξ^2. For a separable (non-entangled) two particle system, the density matrix is defined as

$$\hat{\rho} = |\psi\rangle\langle\psi| = \sum_i p_i\,|\psi_i\rangle^{(1)}\langle\psi_i|^{(1)} \otimes |\psi_i\rangle^{(2)}\langle\psi_i|^{(2)} \tag{3.100}$$

This follows from definitions (3.81) and (3.82). The expectation values that have to be determined in order to find ξ^2 can be found using the last property of the density operator; $\langle\hat{A}\rangle = \mathrm{Tr}\left(\hat{\rho}\hat{A}\right)$ as given in Section 3.3.1.

Instead of working out this expectation value directly, note that the density matrix $\hat{\rho}$ is a convex combination of $|\psi\rangle^{(1)}\langle\psi|^{(1)} \otimes |\psi\rangle^{(2)}\langle\psi|^{(2)}$ because all probabilities satisfy $0 \leq p_i \leq 1$. Now because the inequality holds for pure states, it must also hold for mixed states as the expectation value of these mixed states will be smaller. Namely, a pure state is always an extreme point of the convex set of states [5].

In conclusion, with the squeezing parameter ξ^2 the presence or absence of entanglement can be measured. Namely, $\xi^2 < 1$ is only possible for entangled states. [14]

[14] In a similar manner the entanglement parameter W_{jk} is defined in *Witthaut et al.* [1] to express whether entanglement is present between the two modes j and k.

$$W_{jk} = \Delta Z_{jk}^2 - \langle\hat{n}_j + \hat{n}_k\rangle \tag{3.101}$$

In this equation, $\hat{n}_i$ is the number operator as introduced in Section 3.1.3, applied to mode i. The definition of the number difference operator $\hat{Z}_{jk}$ is the following.

$$\hat{Z}_{jk} = \hat{n}_j - \hat{N}_k \tag{3.102}$$

For a pure state, presence of entanglement of the modes is proven if the entanglement parameter W_{jk} exceeds zero.

3.4 Mean Field Approximation

Mean field theory is applied when the behaviour of a large number of individual components is studied, which all interact with each other. The interaction of these individual components is then approximated by an average effect. This reduces the many-body problem to a single-body problem.

With the mean field approximation, the equations of motion for the amplitudes $c_j = \langle \hat{a_j} \rangle$ are be derived from Heisenberg's equation in *Witthaut et al.* [1] Working this out will show that the phases of these complex amplitudes evolve according to the Kuramoto model. The main results within the derivation will be shown here, but for the details one might want to read Supplementary Note 3 of *Witthait et al.* [1].

Recall Heisenberg's equation of motion (3.16) in Section 3.1.2. When considering the amplitude for the mode n, the equation will be

$$\frac{d\hat{a}_n}{dt} = \frac{i}{\hbar}[\hat{H}, \hat{a}_n] \tag{3.103}$$

The Hamiltonian which describes a quantum many-body system is shown in equation (3.104). It describes L spatially localized modes, $j \in \{1, ..., L\}$, with on-site two-body interactions of energy scale U [1].

$$\hat{H} = \sum_{l=1}^{L} \omega_l \hat{a}_l^\dagger \hat{a}_l + \frac{U}{2} \hat{a}_l^{\dagger 2} \hat{a}_l^2 + \hat{H}_s, \tag{3.104}$$

$$\hat{H}_s = \sum_{j,l=1}^{L} \frac{\tilde{K}_{j,l}}{8} \Big[i(\hat{a}_j^\dagger \hat{a}_l - \hat{a}_j^\dagger \hat{a}_j)(\hat{a}_j^\dagger \hat{a}_j - \hat{a}_l^\dagger \hat{a}_l) + \text{h.c.} \Big]$$

This Hamiltonian will be used to derive the equations of motion for each mode (3.103). The first part of the Hamiltonian shows the contribution by the operators of the mode itself. The last term $\hat{H}_s$ In this can be seen as the interaction-Hamiltonian of this system; it describes the coupling between the different modes. In this sum, if $j = l$, the contribution will be 0. The coupling strength $\tilde{K}_{j,l}$ regulates the amount of contribution of the interaction-Hamiltonian and defines the correlation between different modes.

The dynamics of this (isolated) quantum many-body system are described in *Witthaut et al.* [1]. The system's behaviour can be described in either the weakly or the strongly correlated regime. Between these regimes, the system exhibits a sharp transition. As *Witthaut et al.* [1] states: "When the coupling strengths $\tilde{K}_{j,l}$ exceed a critical value, correlations emerge dynamically and persist independent of the initial state. For small coupling strengths, correlations remain negligible and the modes will gradually dephase."

With this Hamiltonian, Heisenberg's equation of motion (3.103) will be solved for $\hat{a}_n$. With the commutation relations of the creation and annihilation operator as described in Section 3.1.2, the commutators with the Hamiltonian terms can be determined. [15]

$$i\frac{d}{dt}\hat{a}_n = \omega_n \hat{a}_n + U\hat{a}_n^\dagger \hat{a}_n^2 + \sum_{j=1}^{L} \frac{\tilde{K}_{n,j}}{2i} (\hat{a}_j^\dagger \hat{a}_n^2 + \hat{a}_j^\dagger \hat{a}_j^2 - 2\hat{a}_n^\dagger \hat{a}_n \hat{a}_j) \tag{3.107}$$

[15] It is important to note that the annihilation and/or creation operator(s) commute for different modes. Therefore, the terms which include either a commutator between different modes or of the same operator (either two annihilation or two creation operators) are zero. In short, all commutation relations that are needed are those for

Taking the expectation value of this equation yields

$$i\frac{d}{dt}\langle\hat{a}_n\rangle = \omega_n\langle\hat{a}_n\rangle + U\langle\hat{a}_n^\dagger\hat{a}_n^2\rangle + \sum_{j=1}^{L}\frac{\tilde{K}_{n,j}}{2i}(\langle\hat{a}_j^\dagger\hat{a}_n^2\rangle + \langle\hat{a}_j^\dagger\hat{a}_j^2\rangle - 2\langle\hat{a}_n^\dagger\hat{a}_n\hat{a}_j\rangle) \tag{3.108}$$

Note that taking the expectation values of the operators is allowed as the Heisenberg picture is considered. Hence, the state is considered time-independent and the operators hold the system dynamics.

The difficulty for a quantum many-body system now shows; the Heisenberg equations induce an infinite hierarchy of coupled equations for the expectation values [1]. That is, to solve equation (3.108), the expectation values for the third order products have to be determined. These equations will show fifth order products of annihilation and creation operators, and those will show seventh order products, and so on. This can be seen by the fourth order terms in the Hamiltonian (3.104). These add a product of two more operators to each equation in comparison with the previous one. To reduce this infinite number of coupled equations to a finite number of differential equations, the mean field approximation is applied.

In first order mean field, all higher order expectation values are approximated by products of first order ones. In this case, the three-point functions are approximated in terms of one-point functions.

$$\langle\hat{a}_j^\dagger\hat{a}_k\hat{a}_l\rangle \approx \langle\hat{a}_j^\dagger\rangle\langle\hat{a}_k\rangle\langle\hat{a}_l\rangle \tag{3.109}$$

The error in this approximation vanishes as $1/N$, due to which the truncation is generally valid for Bose-Einstein condensates with a lot of particles [1, 33]. The possibility of extending this approximation to second order and therefore truncating the higher order moments in a way to include interaction between the operators is discussed in Section 4.

The mean field equations of motions for first order result in

$$i\frac{d\langle\hat{a}_n\rangle}{dt} = \omega_n\langle\hat{a}_n\rangle + U\langle\hat{a}_n^\dagger\rangle\langle\hat{a}_n\rangle^2 + \sum_{j=1}^{L}\frac{\tilde{K}_{n,j}}{2i}\Big(\langle\hat{a}_j^\dagger\rangle\langle\hat{a}_n\rangle^2 + \langle\hat{a}_j^\dagger\rangle\langle\hat{a}_j\rangle^2 - 2\langle\hat{a}_n^\dagger\rangle\langle\hat{a}_n\rangle\langle\hat{a}_j\rangle\Big) \tag{3.110}$$

All expectation values have now become products of the complex amplitudes c_n, which can be expressed in polar coordinates

$$\langle\hat{a}_n\rangle = c_n = |c_n|e^{-i\phi_n} \tag{3.111}$$

The amplitude and phase are defined as

$$|c_n| = \sqrt{c_n^* c_n} \qquad \text{and} \qquad \phi_n = -\arctan\left(\frac{\mathrm{Im}(c_n)}{\mathrm{Re}(c_n)}\right) \tag{3.112}$$

multiple-boson systems;

$$[\hat{a}_i, \hat{a}_j^\dagger] = \hat{a}_i\hat{a}_j^\dagger - \hat{a}_j^\dagger\hat{a}_i = \delta_{ij} \tag{3.105}$$

and

$$[\hat{a}_i^\dagger, \hat{a}_j^\dagger] = [\hat{a}_i, \hat{a}_j] \tag{3.106}$$

With this representation, the equations of motion (3.110) can be expressed for both the amplitudes and the phases.

$$\frac{d}{dt}|c_n|^2 = -\sum_{j=1}^{L} \tilde{K}_{n,j}(|c_j|^2 - |c_n|^2)|c_j||c_n|\cos(\phi_n - \phi_j) \tag{3.113}$$

$$\frac{d}{dt}\phi_n = \omega_n + U|c_n|^2 + \sum_{j=1}^{L} \frac{\tilde{K}_{n,j}}{2}\frac{|c_j|}{|c_n|}(3|c_n|^2 - |c_j|^2)\sin(\phi_j - \phi_n) \tag{3.114}$$

In the case that all the amplitudes have the same value, that is if $|c_j|^2 = |c_n|^2$ for all j and n in $\{1, 2, ..., L\}$, the amplitudes remain constant. Namely, all terms on the right side of equation (3.113) become zero. The equations for the phase ϕ_n will simplify to

$$\frac{d}{dt}\phi_n = \omega_n + U|c_n|^2 + \sum_{j=1}^{L} \tilde{K}_{n,j}|c_n|^2 \sin(\phi_j - \phi_n) \tag{3.115}$$

which is the celebrated Kuramoto equation for the phases ϕ_n.

Furthermore, the amplitudes are chosen $|c_n|^2 = \frac{N}{L}$ and the coupling parameter is replaced by $K_{n,j} = \tilde{K}_{n,j}N/L$. This substitution corresponds to the number of excitations $N = \sum_{l=1}^{L}|c_l|^2$ being evenly over all L modes. Additionally, the frequency ω_n is substituted by the rescaled frequency $\bar{\omega}_n = \omega_n + U\frac{N}{L}$. The mean field equations of motion for the phase ϕ_n of the complex amplitudes $c_n = \langle \hat{a}_l \rangle$ will then be the differential equations of the Kuramoto model, see equation (2.1).

$$\frac{d\phi_n}{dt} = \bar{\omega}_n + \sum_{j=1}^{L} K_{n,j}\sin(\phi_j - \phi_n) \tag{3.116}$$

4 Beyond First Order Mean Field

In the theoretical research of *Witthait et al.* [1] the mean field approximation was used and only the first order moments were assumed to contribute to the solutions of the equations of motion. In other words, the approximation of equation (3.109) is used. When the amplitudes of these expectation values are assumed to be constant, this results in the equations of the Kuramoto model, see equation (3.116).

When applying mean field approximation to first order only, all correlations between the operators are neglected. The original equation (3.108) includes not only first order moments $\langle \hat{a}_n \rangle$, but also terms with the expectation value of three operators, for example $\langle \hat{a}_n^\dagger \hat{a}_n^2 \rangle$. For these third order moments, all correlations between the operators is reduced to zero when the approximation (3.109) is used. This might yield different results than when all correlations would be taken into account and the original equation (3.108) would be solved.

However, if one would want to solve equation (3.108) without using an approximation, the set of coupled differential equations would be infinitely large. Namely, for the first order moments the third order moments have to be known. When one would solve for these expectation values with three operators, their equations of motion will include terms with the product of five operators. This is due to the higher order terms in the Hamiltonian (3.104). These expectation values then have to be solved for with their equations of motion that includes terms with seven operators, and so forth. The length of the operator products will thus grow infinitely long, and therefore the amount of coupled differential equation will be infinite as well. This could be seen as a chain of equations of which the first equation, which is the main equation we are interested in, can only be solved if the second is known and so on. Additionally, the amount of possible products of a higher number of operators will only be larger as well.

Therefore, the equations have to be truncated. The most simple way to do this would be to approximate all equations with their first order moments, as was done in *Witthaut et al.* [1]. However, as noted above, the correlations between the operators are then neglected fully. To find a solution which might have a higher resemblance with the exact equation (3.108), the second order moments could be added to the mean field approximation. This is where the goal of this research, to apply second order mean field in order to approach the theoretically exact solution more closely, is studied. The second order mean field equations of motion will result into five coupled differential equations for the first and second order moments. These equations will however be more complex and cannot be solved analytically in a similar manner. Therefore, this will not result in the analytical expression for the Kuramoto model.

In this chapter, the derivation of the system of coupled non-linear differential equations will be discussed in Section 4.1.1. These equations are solved numerically in Matlab, and their solutions are shown in Section 4.2. These numerical results will be compared to the solution of *Witthaut et al.* [1]. Their stability will be verified by defining quantum fluctuations beyond mean field in Section 4.3.

4.1 Second Order Mean Field Approximation

The second order mean field approximation includes terms of first and second order only. The higher order moments, the expectation values of the products with more than two annihilation and/or creation operators, must be approximated in terms of these first and second order moments. This is done in the following ways, for products of three or four operators [1, 33]. [16]

$$\langle \hat{A}\hat{B}\hat{C}\rangle \approx \langle \hat{A}\rangle\langle \hat{B}\hat{C}\rangle + \langle \hat{B}\rangle\langle \hat{A}\hat{C}\rangle + \langle \hat{C}\rangle\langle \hat{A}\hat{B}\rangle - 2\langle \hat{A}\rangle\langle \hat{B}\rangle\langle \hat{C}\rangle \tag{4.1}$$

$$\langle \hat{A}\hat{B}\hat{C}\hat{D}\rangle \approx \langle \hat{A}\hat{B}\rangle\langle \hat{C}\hat{D}\rangle + \langle \hat{A}\hat{C}\rangle\langle \hat{B}\hat{D}\rangle + \langle \hat{A}\hat{D}\rangle\langle \hat{B}\hat{C}\rangle - 2\langle \hat{A}\rangle\langle \hat{B}\rangle\langle \hat{C}\rangle\langle \hat{D}\rangle \tag{4.2}$$

Applying this to the initial equation (3.108) yields the following approximation

$$\begin{aligned} i\frac{d}{dt}\langle \hat{a}_n\rangle =& \omega_n\langle \hat{a}_n\rangle + U\Big(\langle \hat{a}_n^\dagger\rangle\langle \hat{a}_n^2\rangle + 2\langle \hat{a}_n\rangle\langle \hat{a}_n^\dagger\hat{a}_n\rangle - 2\langle \hat{a}_n^\dagger\rangle\langle \hat{a}_n\rangle^2\Big) \\ &+ \sum_{j=1}^{L}\frac{\tilde{K}_{n,j}}{2i}\Big(2\langle \hat{a}_j\rangle\langle \hat{a}_j^\dagger\hat{a}_j\rangle - 2\langle \hat{a}_j\rangle\langle \hat{a}_n^\dagger\hat{a}_n\rangle + 2\langle \hat{a}_n\rangle\langle \hat{a}_j^\dagger\hat{a}_n\rangle - 2\langle \hat{a}_n\rangle\langle \hat{a}_n^\dagger\hat{a}_j\rangle \\ &+ \langle \hat{a}_j^\dagger\rangle\langle \hat{a}_j^2\rangle + \langle \hat{a}_j^\dagger\rangle\langle \hat{a}_n^2\rangle - 2\langle \hat{a}_n^\dagger\rangle\langle \hat{a}_j\hat{a}_n\rangle - 2\langle \hat{a}_j^\dagger\rangle\langle \hat{a}_j\rangle^2 - 2\langle \hat{a}_j^\dagger\rangle\langle \hat{a}_n\rangle^2 + 4\langle \hat{a}_n^\dagger\rangle\langle \hat{a}_j\rangle\langle \hat{a}_n\rangle\Big) \end{aligned} \tag{4.3}$$

It can be noted that there are various new expectation values for which the equation of motion will have to be determined in order to solve (4.3). The additional equations that are needed to solve this new system are the time derivatives for the following expectation values $\langle \hat{a}_n^2\rangle$, $\langle \hat{a}_n^\dagger\hat{a}_n\rangle$, $\langle \hat{a}_n\hat{a}_m\rangle$ with $n \neq m$ and $\langle \hat{a}_n^\dagger\hat{a}_m\rangle$ with $n \neq m$. These are given in Section 4.1.1. The other possible combinations of annihilation and creation operators are either the same as or can be deduced from the products above. For example, as *Witthaut et al.* [1] used already, the following can be used for the differential equation for the creation operator for mode n.

$$\langle \hat{a}_n^\dagger\rangle = \langle \hat{a}_n\rangle^* \tag{4.4}$$

In words, the expectation value of the creation operator is the complex conjugate of the annihilation operator. For $\langle \hat{a}_n^{\dagger 2}\rangle$ and $\langle \hat{a}_n^\dagger\hat{a}_m^\dagger\rangle$ similar relations can be used.

$$\langle \hat{a}_n^{\dagger 2}\rangle = \langle \hat{a}_n^2\rangle^* \tag{4.5}$$

$$\langle \hat{a}_n^\dagger\hat{a}_m^\dagger\rangle = \langle \hat{a}_n\hat{a}_m\rangle^* \qquad n \neq m \tag{4.6}$$

Furthermore, the equation of $\langle \hat{a}_n\hat{a}_n^\dagger\rangle$ can be shown to be equal to the differential equation for $\langle \hat{a}_n^\dagger\hat{a}_n\rangle$. Namely, from the commutation relation (3.12) it can be deduced that

$$\hat{a}_n^\dagger\hat{a}_n = \hat{a}_n\hat{a}_n^\dagger - 1 \tag{4.7}$$

Substituting this into a time derivative will give the same result, as this constant -1 will fall out.

Note that the operators for different modes commute and can therefore be re-ordered arbitrarily. As a result, $\langle \hat{a}_n\hat{a}_m\rangle = \langle \hat{a}_m\hat{a}_n\rangle$ and $\langle \hat{a}_n^\dagger\hat{a}_m\rangle = \langle \hat{a}_m\hat{a}_n^\dagger\rangle$ for $n \neq m$. Therefore only one equation suffices for each combination of operators for n and m, regardless of the order that they appear in.

[16] As only first order mean field was considered in *Witthaut et al.* [1], the second order equations of motion are derived by hand with he approximations (4.1) and (4.2). These approximations were found in *Tikhonenkov et al.* [33], the source that [1] cited to justify the first order mean field. The truncations are based on the Hartree-Fock-Bogoliubov theory and can be applied to condensates and weakly interacting Bose gases [19, 33].

The number of equations will be higher for a larger set of modes, as equations of motion are needed for each mode. The amount of distinct equations will however not be dependent on the number of modes assumed, as the equation is of the same form for each mode (or combination of modes) because the modes are assumed to be identical. Therefore the only effect of a higher number of modes is that the system will have to be solved with a higher number of equations numerically, but these equations are all of the same shape.

A few checks can be done for each equation of motion that is computed. In the initial equation (3.108), the contribution of the interaction Hamiltonian $\hat{H}_s$ will reduce to zero for the term $j = n$ in the summation. This can be seen from the definition of the Hamiltonian (3.104) as well as by filling in $j = n$ in the equation (3.108). This physically means that there is only coupling present between different modes. The contribution for the mode itself is entirely expressed in the first part of the Hamiltonian. The fact that this term of the sum should reduce to zero can be used as the first check for each of the (approximated) equations. Also, each equation should have 10 negative and 10 positive terms in the terms that follow from the interaction part of the Hamiltonian $\hat{H}_s$. Furthermore, the the order of the terms can be easily checked, as well as the number of creation versus annihilation operators. The summations over j for either $K_{n,j}$ or $K_{m,j}$ should be the same (but m substituted for n or the other way around). Lastly, the symmetry in the commutation relations has to be visible in the equations as well.

4.1.1 Equations of Motion

In order to solve equation (4.3) (for different modes n), the equations of motion for $\langle \hat{a}_n^2 \rangle$, $\langle \hat{a}_n^\dagger \hat{a}_n \rangle$, $\langle \hat{a}_n \hat{a}_m \rangle$ with $n \neq m$ and $\langle \hat{a}_n^\dagger \hat{a}_m \rangle$ with $n \neq m$ have to be determined. With the use of various commutation relations, the equations of motion for (second order) products of annihilation and creation operators (for either different or the same modes) are derived with the Heisenberg equation of motion (3.16).

The commutation relations that were used are

$$[\hat{a}_n, \hat{a}_j^\dagger \hat{a}_j] = \delta_{nj} \hat{a}_n \tag{4.8}$$

$$[\hat{a}_n^\dagger, \hat{a}_j^\dagger \hat{a}_j] = -\delta_{nj} \hat{a}_n^\dagger \tag{4.9}$$

$$[\hat{a}_n, \hat{a}_j^{\dagger 2} \hat{a}_j^2] = 2\delta_{nj} \hat{a}_n^\dagger \hat{a}_n^2 \tag{4.10}$$

$$[\hat{a}_n^\dagger, \hat{a}_j^{\dagger 2} \hat{a}_j^2] = -2\delta_{nj} \hat{a}_n^{\dagger 2} \hat{a}_n \tag{4.11}$$

$$[\hat{a}_n, \hat{a}_j^\dagger \hat{a}_l \hat{a}_j^\dagger \hat{a}_j] = \delta_{nj} \hat{a}_l \hat{a}_j^\dagger \hat{a}_j + \delta_{nj} a_j^\dagger \hat{a}_l \hat{a}_j \tag{4.12}$$

$$[\hat{a}_n^\dagger, \hat{a}_j^\dagger \hat{a}_l \hat{a}_j^\dagger \hat{a}_j] = -\delta_{nl} \hat{a}_j^{\dagger 2} \hat{a}_j - \delta_{nj} \hat{a}_j^\dagger \hat{a}_l \hat{a}_j^\dagger \tag{4.13}$$

$$[\hat{a}_n, \hat{a}_j^\dagger \hat{a}_l \hat{a}_l^\dagger \hat{a}_l] = \delta_{nj} \hat{a}_l \hat{a}_l^\dagger \hat{a}_l + \delta_{nl} \hat{a}_k^\dagger \hat{a}_k^2 \tag{4.14}$$

$$[\hat{a}_n^\dagger, \hat{a}_j^\dagger \hat{a}_l \hat{a}_l^\dagger \hat{a}_l] = -\delta_{nl} \hat{a}_j^\dagger \hat{a}_l^\dagger \hat{a}_l - \delta_{nl} \hat{a}_j^\dagger \hat{a}_l \hat{a}_l^\dagger \tag{4.15}$$

These are all derived from equations (3.105) and (3.106), see footnote 15, which boil down to the elementary commutation relation (3.12).

After computing the equations of motion, the second order mean field approximations (4.1) and (4.2) are applied. This results in the final second order mean field equations of motion; a system of five coupled differential equations. Equation (4.3) is the first one, and the expectation values that appear in any of the five coupled equations are expressed in one of the other equations.

$$
\begin{aligned}
i\frac{d}{dt}\langle\hat{a}_n^2\rangle =& 2\omega_n\langle\hat{a}_n^2\rangle + U\Big(2\langle\hat{a}_n^\dagger\rangle\langle\hat{a}_n^2\rangle + 4\langle\hat{a}_n\rangle\langle\hat{a}_n^\dagger\hat{a}_n\rangle - 4\langle\hat{a}_n\rangle^2\langle\hat{a}_n^\dagger\rangle\Big) \\
&+ \sum_{j=1}^{L}\frac{\tilde{K}_{n,j}}{2i}\Big(2\langle\hat{a}_j^2\rangle\langle\hat{a}_j^\dagger\hat{a}_n\rangle + 6\langle\hat{a}_n^2\rangle\langle\hat{a}_j^\dagger\hat{a}_n\rangle - 4\langle\hat{a}_n^2\rangle\langle\hat{a}_n^\dagger\hat{a}_j\rangle + 4\langle\hat{a}_j^\dagger\hat{a}_j\rangle\langle\hat{a}_j\hat{a}_n\rangle \\
&- 8\langle\hat{a}_n^\dagger\hat{a}_n\rangle\langle\hat{a}_j\hat{a}_n\rangle - 4\langle\hat{a}_j^\dagger\rangle\langle\hat{a}_j\rangle^2\langle\hat{a}_n\rangle - 4\langle\hat{a}_j^\dagger\rangle\langle\hat{a}_n\rangle^3\langle + 8\langle\hat{a}_n^\dagger\rangle\langle\hat{a}_j\rangle\langle\hat{a}_n\rangle^2\Big)
\end{aligned} \tag{4.16}
$$

$$
\begin{aligned}
i\frac{d}{dt}\langle\hat{a}_n^\dagger\hat{a}_n\rangle =& U\Big(\langle\hat{a}_n^\dagger\rangle\langle\hat{a}_n^2\rangle + 2\langle\hat{a}_n\rangle\langle\hat{a}_n^\dagger\hat{a}_n\rangle - 2\langle\hat{a}_n^\dagger\rangle\langle\hat{a}_n^\dagger\hat{a}_n\rangle - \langle\hat{a}_n\rangle\langle\hat{a}_n^{\dagger 2}\rangle - 2\langle\hat{a}_n^\dagger\rangle\langle\hat{a}_n\rangle^2 \\
&+ 2\langle\hat{a}_n^\dagger\rangle^2\langle\hat{a}_n\rangle\Big) + \sum_{j=1}^{L}\frac{\tilde{K}_{n,j}}{2i}\Big(+ 2\langle\hat{a}_j^\dagger\hat{a}_j\rangle\langle\hat{a}_j^\dagger\hat{a}_n\rangle + 2\langle\hat{a}_j^\dagger\hat{a}_j\rangle\langle\hat{a}_n^\dagger\hat{a}_j\rangle \\
&- 2\langle\hat{a}_n^\dagger\hat{a}_n\rangle\langle\hat{a}_j^\dagger\hat{a}_n\rangle - 2\langle\hat{a}_n^\dagger\hat{a}_n\rangle\langle\hat{a}_n^\dagger\hat{a}_j\rangle - 2\langle\hat{a}_n^{\dagger 2}\rangle\langle\hat{a}_j\hat{a}_n\rangle + 2\langle\hat{a}_j^{\dagger 2}\rangle\langle\hat{a}_j\hat{a}_n\rangle \\
&- \langle\hat{a}_n^2\rangle\langle\hat{a}_n^\dagger\hat{a}_j^\dagger\rangle + \langle\hat{a}_j^2\rangle\langle\hat{a}_n^\dagger\hat{a}_j^\dagger\rangle - 2\langle\hat{a}_j^\dagger\rangle^2\langle\hat{a}_n\rangle\langle\hat{a}_j\rangle + 2\langle\hat{a}_n^\dagger\rangle^2\langle\hat{a}_n\rangle\langle\hat{a}_j\rangle \\
&- 2\langle\hat{a}_n^\dagger\rangle\langle\hat{a}_j^\dagger\rangle\langle\hat{a}_j\rangle^2 + 2\langle\hat{a}_n^\dagger\rangle\langle\hat{a}_j^\dagger\rangle\langle\hat{a}_n\rangle^2\Big)
\end{aligned} \tag{4.17}
$$

For different modes ($n \neq m$), when applying the second order mean field approximation, the equations of motion are the following.

$$
\begin{aligned}
i\frac{d}{dt}\langle\hat{a}_n\hat{a}_m\rangle =& (\omega_n+\omega_m)\langle\hat{a}_n\hat{a}_m\rangle + U\Big(\langle\hat{a}_n^2\rangle\langle\hat{a}_n^\dagger\hat{a}_m\rangle + \langle\hat{a}_m^2\rangle\langle\hat{a}_m^\dagger\hat{a}_n\rangle \\
&+ 2\langle\hat{a}_n^\dagger\hat{a}_n\rangle\langle\hat{a}_n\hat{a}_m\rangle + 2\langle\hat{a}_m^\dagger\hat{a}_m\rangle\langle\hat{a}_n\hat{a}_m\rangle - 2\langle\hat{a}_n\rangle^2\langle\hat{a}_m\rangle\langle\hat{a}_n^\dagger\rangle - 2\langle\hat{a}_m\rangle^2\langle\hat{a}_n\rangle\langle\hat{a}_m^\dagger\rangle\Big) \\
&\sum_{j=1}^{L}\frac{\tilde{K}_{n,j}}{2i}\Big(2\langle\hat{a}_j^\dagger\hat{a}_j\rangle\langle\hat{a}_j\hat{a}_m\rangle - 2\langle\hat{a}_n^\dagger\hat{a}_n\rangle\langle\hat{a}_j\hat{a}_m\rangle + 2\langle\hat{a}_j^\dagger\hat{a}_n\rangle\langle\hat{a}_n\hat{a}_m\rangle \\
&- 2\langle\hat{a}_n^\dagger\hat{a}_j\rangle\langle\hat{a}_n\hat{a}_m\rangle - 2\langle\hat{a}_n^\dagger\hat{a}_m\rangle\langle\hat{a}_n\hat{a}_j\rangle + \langle\hat{a}_j^\dagger\hat{a}_m\rangle\langle\hat{a}_j^2\rangle + \langle\hat{a}_j^\dagger\hat{a}_m\rangle\langle\hat{a}_n^2\rangle \\
&- 2\langle\hat{a}_j^\dagger\rangle\langle\hat{a}_j\rangle^2\langle\hat{a}_m\rangle - 2\langle\hat{a}_j^\dagger\rangle\langle\hat{a}_n\rangle^2\langle\hat{a}_m\rangle + 4\langle\hat{a}_n^\dagger\rangle\langle\hat{a}_j\rangle\langle\hat{a}_n\rangle\langle\hat{a}_m\rangle\Big) \\
&+ \sum_{j=1}^{L}\frac{\tilde{K}_{m,j}}{2i}\Big(2\langle\hat{a}_j^\dagger\hat{a}_j\rangle\langle\hat{a}_j\hat{a}_n\rangle - 2\langle\hat{a}_m^\dagger\hat{a}_m\rangle\langle\hat{a}_j\hat{a}_n\rangle + 2\langle\hat{a}_j^\dagger\hat{a}_m\rangle\langle\hat{a}_n\hat{a}_m\rangle \\
&- 2\langle\hat{a}_m^\dagger\hat{a}_j\rangle\langle\hat{a}_n\hat{a}_m\rangle - 2\langle\hat{a}_m^\dagger\hat{a}_n\rangle\langle\hat{a}_m\hat{a}_j\rangle + \langle\hat{a}_j^\dagger\hat{a}_n\rangle\langle\hat{a}_j^2\rangle + \langle\hat{a}_j^\dagger\hat{a}_n\rangle\langle\hat{a}_m^2\rangle \\
&- 2\langle\hat{a}_j^\dagger\rangle\langle\hat{a}_j\rangle^2\langle\hat{a}_n\rangle - 2\langle\hat{a}_j^\dagger\rangle\langle\hat{a}_m\rangle^2\langle\hat{a}_n\rangle + 4\langle\hat{a}_m^\dagger\rangle\langle\hat{a}_j\rangle\langle\hat{a}_n\rangle\langle\hat{a}_m\rangle\Big)
\end{aligned} \tag{4.18}
$$

$$
\begin{aligned}
i\frac{d}{dt}\langle \hat{a}_n^\dagger \hat{a}_m\rangle =&(\omega_m-\omega_n)\langle \hat{a}_n^\dagger \hat{a}_m\rangle + U\Big(-\langle \hat{a}_n^{\dagger 2}\rangle\langle \hat{a}_n\hat{a}_m\rangle + \langle \hat{a}_m^2\rangle\langle \hat{a}_n^\dagger \hat{a}_m^\dagger\rangle \\
&-2\langle \hat{a}_n^\dagger \hat{a}_n\rangle\langle \hat{a}_n^\dagger \hat{a}_m\rangle + 2\langle \hat{a}_m^\dagger \hat{a}_m\rangle\langle \hat{a}_n^\dagger \hat{a}_m\rangle + 2\langle \hat{a}_n^\dagger\rangle^2\langle \hat{a}_n\rangle\langle \hat{a}_m\rangle - 2\langle \hat{a}_n^\dagger\rangle\langle \hat{a}_m^\dagger\rangle\langle \hat{a}_m\rangle^2\Big) \\
&\sum_{j=1}^{L}\frac{\tilde{K}_{n,j}}{2i}\Big(2\langle \hat{a}_j^\dagger \hat{a}_j\rangle\langle \hat{a}_m^\dagger \hat{a}_j\rangle - 2\langle \hat{a}_n^\dagger \hat{a}_n\rangle\langle \hat{a}_m^\dagger \hat{a}_j\rangle + 2\langle \hat{a}_m^\dagger \hat{a}_n\rangle\langle \hat{a}_j^\dagger \hat{a}_n\rangle - 2\langle \hat{a}_m^\dagger \hat{a}_n\rangle\langle \hat{a}_n^\dagger \hat{a}_j\rangle \\
&+\langle \hat{a}_j^2\rangle\langle \hat{a}_j^\dagger \hat{a}_m^\dagger\rangle + \langle \hat{a}_n^2\rangle\langle \hat{a}_j^\dagger \hat{a}_m^\dagger\rangle - 2\langle \hat{a}_j\hat{a}_n\rangle\langle \hat{a}_j^\dagger \hat{a}_m^\dagger\rangle \\
&-2\langle \hat{a}_j^\dagger\rangle\langle \hat{a}_m^\dagger\rangle\langle \hat{a}_j\rangle^2 - 2\langle \hat{a}_j^\dagger\rangle\langle \hat{a}_m^\dagger\rangle\langle \hat{a}_n\rangle^2 + 4\langle \hat{a}_n^\dagger\rangle\langle \hat{a}_m^\dagger\rangle\langle \hat{a}_n\rangle\langle \hat{a}_j\rangle\Big) \\
&+\sum_{j=1}^{L}\frac{\tilde{K}_{m,j}}{2i}\Big(2\langle \hat{a}_j^\dagger \hat{a}_j\rangle\langle \hat{a}_n^\dagger \hat{a}_j\rangle - 2\langle \hat{a}_m^\dagger \hat{a}_m\rangle\langle \hat{a}_j^\dagger \hat{a}_n\rangle + 2\langle \hat{a}_m^\dagger \hat{a}_n\rangle\langle \hat{a}_m^\dagger \hat{a}_j\rangle - 2\langle \hat{a}_m^\dagger \hat{a}_n\rangle\langle \hat{a}_j^\dagger \hat{a}_m\rangle \\
&+\langle \hat{a}_j^2\rangle\langle \hat{a}_j\hat{a}_n\rangle + \langle \hat{a}_m^2\rangle\langle \hat{a}_j\hat{a}_n\rangle - 2\langle \hat{a}_j^\dagger \hat{a}_n^\dagger\rangle\langle \hat{a}_n\hat{a}_m\rangle \\
&-2\langle \hat{a}_j^\dagger\rangle^2\langle \hat{a}_n^\dagger\rangle\langle \hat{a}_j\rangle - 2\langle \hat{a}_m^\dagger\rangle^2\langle \hat{a}_n\rangle\langle \hat{a}_j\rangle + 4\langle \hat{a}_j^\dagger\rangle\langle \hat{a}_m^\dagger\rangle\langle \hat{a}_n\rangle\langle \hat{a}_m\rangle\Big)
\end{aligned}
\tag{4.19}
$$

Equations (4.3) and (4.16) - (4.19) will have to be solved to find the behaviour of the total system. Analytically, this is not possible any longer as the equations have become too complex. Therefore, the equations will be solved numerically in Matlab.

4.2 Numerical Results

The new equations of motion (4.3) and (4.16) - (4.19) cannot be solved analytically. Therefore, these equations are numerically solved in Matlab. As stated before, the higher the amount of modes considered in the system, the higher the number of equations that have to be solved. Therefore, the most simple system of two modes is solved for first. To solve for $\langle \hat{a}_1 \rangle$ and $\langle \hat{a}_2 \rangle$, a system of nine coupled and non-linear differential equations is defined (one for each operator, and different modes yield different operators although they have the same form of equations). These differential equations are solved simultaneously in small time steps, such that the dynamics of the system can be studied. The code for the numerical solution is included in Appendix A.

To be able to compare the results to the first order mean field solution, this system of equations is solved numerically as well. This will be a system of two differential equations, one for each mode. These equations are defined as (3.110).

The input values ω_i, U and K are chosen the same for both the first and second order mean field approximations. Therefore, the only difference between the two solutions can be a consequence of the different approximation, thus of the interaction between the various modes. The use of second order moments instead of first order moments is intended to be the only difference between the two numerical solutions. However, when using the second order moments, a higher number of equations has to be solved. As the system is more complex, the numerical errors might effect the system more strongly. Moreover, as the calculations were done by hand, small errors might be more probable to occur.

The numerical solutions for both the first and second order were unstable when using the Runge-Kutta method; for a longer integration time, the expectation values would increase rapidly. The two-mode system seemed unstable for both first and second order, which showed for larger time spans. With a different time-integration method however, for example the trapezoidal method or the Verlet algorithm, the first order mean field solutions were found to be stable. The numerical results for first and second order mean field will be discussed in Sections 4.2.1 and 4.2.2.

4.2.1 First Order Mean Field

The numerical solution for the first order mean field equations can be found for various time spans, parameter choices and initial conditions. The Runge-Kutta formula for numerical integration was used first to find the solutions for (3.110) in case of two modes. For very long time spans or higher values for U, K or ω_i, the amplitudes of the operator expectations $c_1 = \langle \hat{a}_1 \rangle$ and $c_2 = \langle \hat{a}_2 \rangle$ grow to high values such that the numerical integration stops. The solution thus seems to be unstable for long times or a high value of the parameters.

For a shorter integration time, or lower values for U and K in equation (3.110), the dynamics of the system can be studied and compared to the theoretical expectations and the solutions of *Witthaut et al.* [1]. In Figures 7 and 8, the amplitude of the (complex valued) expectation value of the creation operator $|c_i|^2 = |\langle \hat{a}_i \rangle|^2$ is plotted versus time for each mode i. Figure 7 shows the behaviour for very short times, and thus shows the very first dynamics of the system and the first part of Figure 8, which shows a longer integration time.

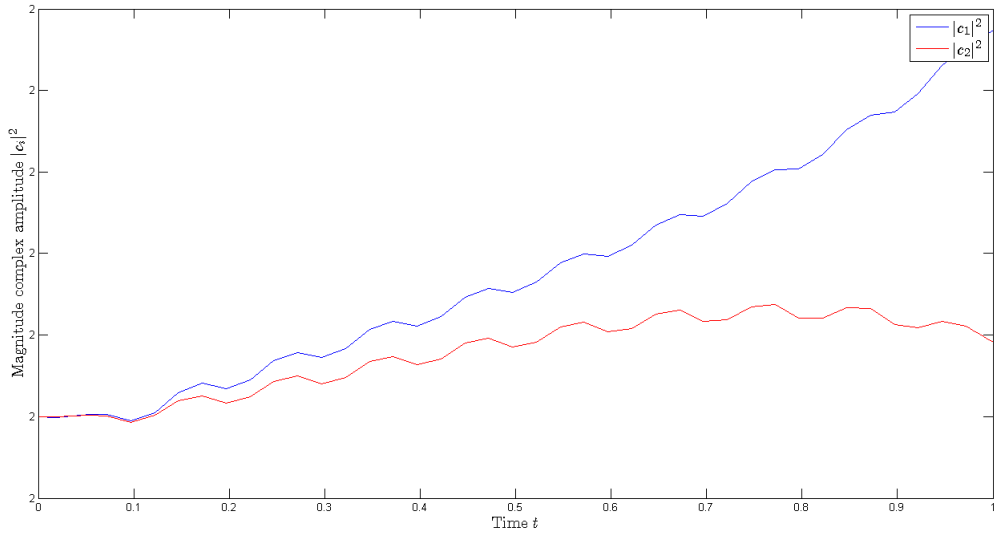

Figure 7: Matlab plot of the modulus of the amplitudes of the (complex) expectation value $\langle \hat{a}_1 \rangle = c_1$ and $\langle \hat{a}_2 \rangle = c_2$ versus time, by numerical integration (Appendix A) of the first order mean field equations of motion with the Runge-Kutta method. The input parameters were $U = 0.5$, $K = 0.5$, $\omega_1 = 0.6$ and $\omega_2 = 0.8$. The initial conditions were chosen $c_1 = c_2 = 2i$ at $t = 0$.

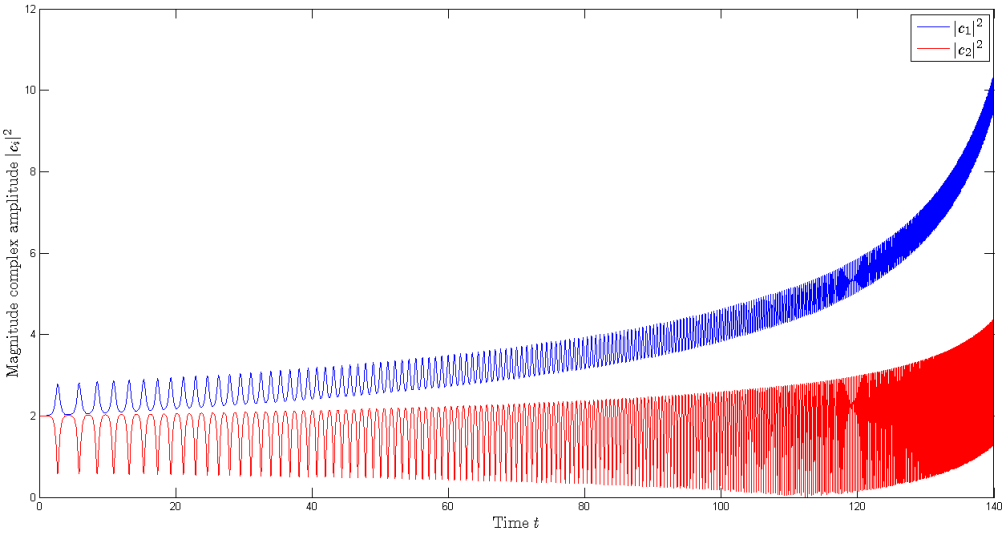

Figure 8: Matlab plot of the modulus of the amplitudes of the (complex) expectation value $\langle \hat{a}_1 \rangle = c_1$ and $\langle \hat{a}_2 \rangle = c_2$ versus time, by numerical integration (Appendix A) of the first order mean field equations of motion with the Runge-Kutta method. The input parameters were $U = 0.5$, $K = 0.5$, $\omega_1 = 0.6$ and $\omega_2 = 0.8$. The initial conditions were chosen $c_1 = c_2 = 2i$ at $t = 0$.

A few things can be noticed in these plots. First, for both modes the expectation values of the annihilation operator indeed grow in amplitude exponentially. Secondly, the amplitudes c_n oscillate in time and there is a clear difference in amplitude between mode 1 and mode 2, whereas the only difference in their equations was their natural frequency ω_i. Furthermore, the oscillations of the amplitudes seem to be mirrored; when the amplitude of c_1 increases the amplitude of c_2 decreases and the other way around. These observations could be explained by looking at the system as a non-linear oscillator, although the values of c_1 and c_2 are complex because of which the comparison does not hold exactly. When both the initial conditions and the natural frequencies were however set to the same value, both modes show exactly the same behaviour (as could be expected). This is one of the checks to exclude the possibility that cause for unexpected behaviour is in improper implementation of the equations of motion.

The phase plots for the complex amplitudes $\langle \hat{a}_i \rangle = c_i$ were not as insightful and are therefore not included in this report. When the amplitudes do not stay constant, the phase of these complex values cannot be easily compared with the phase in the sense of the Kuramoto model. For longer times, the phase plot showed a lot of oscillations due to the jump in argument from 0 to 2π, which undermined the ability to interpret the plot correctly.

As the most important result is the instability of the numerical results, the possible causes are elaborated on. These could be either in the system of equations itself or in the numerical time integration.

On the one hand, one might not expect the system of equations to be unstable as its results in *Witthaut et al.* [1] do not show any instability. In this paper however, for this problem only the theoretical solutions were given and those were only analytically computed under the assumption that the amplitude $|c_i|$ would be constant for each mode. In other words, on the manifold where

$$\frac{d|c_n|^2}{dt} = 0 \tag{4.20}$$

the Kuramoto equation would follow as the differential equations for the phases of these amplitudes ϕ_n [1]. Equation (4.20) holds if the amplitudes of all modes have the same value, thus for two modes if [1]

$$|c_1|^2 = |c_2|^2 \tag{4.21}$$

The initial conditions used for the numerical solutions did satisfy this characteristic, as they were both taken exactly the same (complex) value. It seems from the results in Figure 8 however, that the system does not stay on the (toric) manifold where (4.20) and (4.21) hold [1].

If the instability of the numerical results were assumed to be caused by an unstable system of equations, the most likely explanation for the instability of the first order mean field equations is the limitation of two modes only. The truncation to first order moments is generally valid for Bose-Einstein condensates with a high number of modes, as the error decreases as $1/N$ [1, 33]. The minimal value of two modes might not satisfy the mean field equations close enough, due to which the approximation of the system is unstable. It could therefore be that the theoretical equations are stable, but that the numerical execution for two modes only will be unstable.

On the other hand, the exponential growth of the parameters for large times or high-valued parameters might be caused by errors in the numerical integration. This is quite likely, as even the harmonic oscillator is unstable when using the Runge-Kutta 4 method for integration. This can be explained by the eigenvalues of the system. As these are purely imaginary in case of

the harmonic oscillator, the real part should be zero. In the numerical values however, this real part will be close to zero but can be either slightly positive or negative. A positive real part of the eigenvalue will cause the system to blow up, which will show in the results. A solution to this problem might be using the Verlet integration algorithm [17] , or using a different numerical integration method.

It was checked first whether the complex integration was causing errors in the numerical process by separating the complex differential equations into a real and imaginary part. This was shown to have no effect however, as the numerical solutions were the same.

Moreover, it could be that the differential equations show stiffness, such that certain numerical methods are numerically unstable. Stiff differential equations describe problems that exhibit transients [36]. Their solutions are the sum of high frequency oscillations and a decaying function, which tends to an equilibrium value. Due to these high frequency oscillations, explicit time-integration methods show problems. Namely, the time step of an explicit time-integration method has to be chosen small enough to show these fast oscillations. However, with respect to the accuracy of the quasi-stationary solution, larger time steps could be taken. Therefore, for solutions which show both high frequency oscillations and a long-term quasi-stable solutions, the stability condition restricts the time step more than the accuracy requirement [36]. Implicit time-integration methods must be used instead, as these are unconditionally stable and thus impose no restrictions on the step size. An example of such an implicit method which is unconditionally stable, the trapezoidal method could be studied. This method is indeed unconditionally stable when all eigenvalues have a non-positive real part whereas the Runge-Kutta methods are only stable for the region shown in Figure 9.

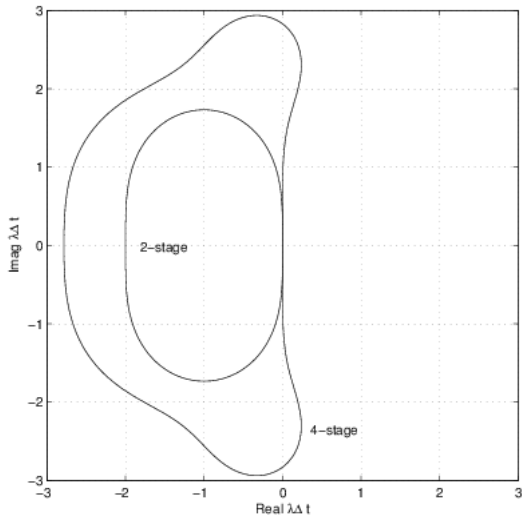

Figure 9: Stability region for the Runge-Kutta time-integration method for second and fourth order [25].

As the numerical results did indeed show high frequency oscillations as well as different long-term

[17]The Verlet integration method is a numerical method used to integrate Newton's equations of motion. It provides good numerical stability and can be seen as an explicit central difference method. More on this algorithm can be read in *Verlet* [35] or *Hairer et al.* [22].

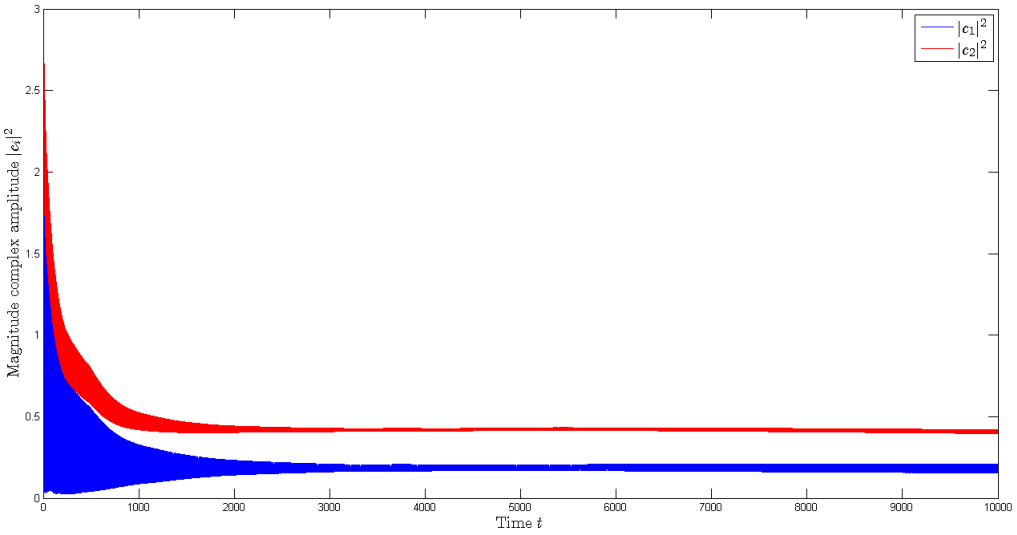

Figure 10: Matlab plot of the modulus of the amplitudes of the (complex) expectation value $\langle \hat{a}_1 \rangle = c_1$ and $\langle \hat{a}_2 \rangle = c_2$ versus time, by numerical integration with the trapezoidal rule (Appendix A). The input parameters were $U = 0.5$, $K = 0.5$, $\omega_1 = 0.6$ and $\omega_2 = 0.8$. The initial conditions were chosen $c_1 = c_2 = 2i$ at $t = 0$.

behaviour, the instability of the Runge-Kutta time-integration method might have caused the instability in the numerical results for the first order mean field solutions, shown in Figures 7 and 11. To check whether this is the case, an implicit numerical integration method is used to solve the system of differential equations. The results of integration with the trapezoidal method are shown in Figure 10.

It can be noted that there was indeed a cause for instability in the numerical integration as the integration with the implicit trapezoidal method shows no ongoing increase in magnitude of the complex amplitude. Its values oscillate strongly in the beginning, but seem to converge to a finite value for longer times. A high frequent oscillation is still present however, but the amplitude of this oscillation is small. This oscillation does still cause the phase plots to be incomparable to the Kuramoto phase oscillations. Namely, the solutions for the magnitudes of the complex amplitude are not constant and thus do not satisfy equation (4.20).

Further research is needed on the (in)stability of the time-integration methods used to solve the equations of motion for the mean field approximation. The amplification factor of the system and the eigenvalues of the Jacobian matrix could give more insight in the propagation of numerical errors. The Verlet algorithm could be studied and applied to the system of differential equations, as this would provide a stable numerical integration method.

4.2.2 Second Order Mean Field

The second order mean field equations of motion were solved numerically as well. Nine coupled differential equations were implemented in Matlab en solved for using the Runge-Kutta as well as the trapezoidal time-integration again, see Appendix A.

Where the first order solutions could be computed for longer times, the second order solution grows even more rapidly and can therefore only be numerically integrated for very short time spans. The results of this time integration can be seen in Figure 11. Notice that the plot has a logarithmic y-axis and is thus scaled differently from the earlier plots. Unfortunately, no solutions were found which could give some insight in the new approximation of the mean field equations of motion. It can therefore not be concluded what the effect is of extending the mean field approximation to second order, for a set of two modes.

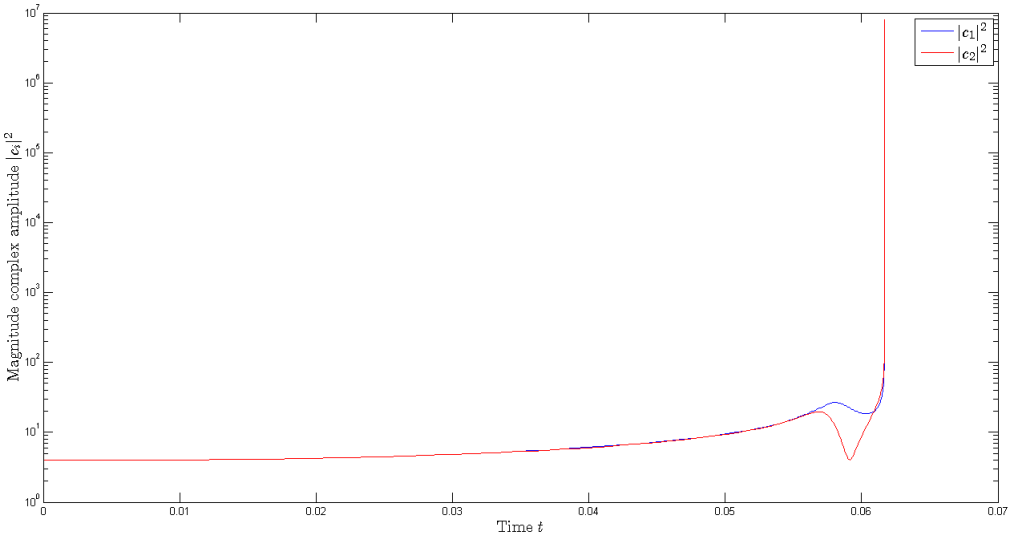

Figure 11: Matlab plot of the modulus of the amplitudes of the (complex) expectation value $\langle \hat{a}_1 \rangle = c_1$ and $\langle \hat{a}_2 \rangle = c_2$ versus time, by numerical integration (Appendix A) of the second order mean field equations of motion using the trapezoidal method. The input parameters were $U = 0.5$, $K = 0.5$, $\omega_1 = 0.6$ and $\omega_2 = 0.8$. The initial conditions were chosen $c_1 = c_2 = 2i$ at $t = 0$. The time integration has stopped early because the magnitude of the complex amplitude has reached too high values.

The fact that for second order, the amplitude of the complex expectation values increases at an even faster rate is remarkable. Both the Runge-Kutta integration as well as the trapezoidal method give unstable solutions. This was striking as this new approximation was expected to resemble the theoretical solution of equation (3.108) more closely, and was therefore not expected to have such a large influence. In fact, the second order influences were hypothetically assumed to be small as the first order mean field approximation was said to be justified. This difference could however be due to the use of only two modes. Furthermore, when the first order solution was found to show instability as well, the second order was naturally predicted to be unstable as well. With more equations (which all have roughly the same form as the first order equations), the unstable effects are only enlarged. Even more fundamentally, the correctness of the

second order mean field equations of motion could be questioned. These were based on equations (4.1) and (4.2) from *Tikhonenkov et al.* [33]. The justification for this way of truncation includes models, such as the Hartree-Fock-Bogoliubov theory, which were not studied for this thesis. Therefore, further research into this branch of quantum mechanics is needed. Also, the second order equations of motion were derived by hand and thereafter implemented in Matlab manually. Errors could have slipped in, although multiple checks have been done to avoid this (see Section 3.4). The numerical time integration must again be investigated into further detail, such that the integration can be excluded as a cause for instability in the second order mean field equations of motion.

In Section 4.3, the difference between the first and second order mean field solutions are studied by looking at quantum fluctuations beyond mean field.

4.3 Quantum Fluctuations

To find out whether the mean field approximation is indeed unstable when the system is limited to two modes only, the dynamics beyond mean field are studied. If these can be shown to be unstable, the growth in amplitude of the expectation values would be explained by the instability of the mean field approximation.

To do so, the dynamics of quantum fluctuations beyond mean field are studied. This is similar to the approach followed in *Witthaut et al.* [1] to describe system the beyond mean field. The bosonic annihilation operators are decomposed into two parts. The first part is the condensate mode c_n, which is the averaged effect of the condensate [1]. This mode is described by the expectation value of the annihilation operator in (first order) mean field $\langle \hat{a}_n \rangle$. The second part is the operator for the remaining quantum fluctuations $\hat{b}_n$. This results in the following ansatz:

$$\hat{a}_n = c_n + \hat{b}_n \tag{4.22}$$

For the creation operator, the ansatz is analogously

$$\hat{a}_n^\dagger = c_n^* + \hat{b}_n^\dagger \tag{4.23}$$

In these equations, the condensate mode c_n or c_n^* are given by the expectation value of $\hat{a}_n$ and $\hat{a}_n^\dagger$ respectively, in the absence of any correlations between the condensate operators (and thus in first order mean field). This way of describing the system resembles perturbation theory, as the condensate mode system can be solved analytically and the perturbation of the quantum fluctuations is assumed to be small.

In an almost pure condensate with N atoms, c_n is of order $\sqrt{N}$ whereas the fluctuations $\hat{b}_n$ are of order 1 [1]. This shows that for a high number of modes, the quantum fluctuations can indeed be neglected, which results in the mean field solution. For two modes only however, the orders of c_n and $\hat{b}_n$ are similar.

If the quantum fluctuations $\hat{b}_n$ are high and cannot be neglected, the (first order) mean field approximation does not resemble the theoretical solution for the expectation value of $\hat{a}_n$ correctly. Namely, in the first order mean field approximation, the expectation value of the annihilation operator is assumed to be exactly c_n and $\hat{b}_n$ is set to zero.

To find out the influence of the quantum fluctuations, the difference between the first and second order mean field equations is studied. Equations (4.22) and (4.23) are substituted in the first and second order mean field equations of motion, equations (3.110) and (4.3) respectively. In first order mean field however, the fluctuations do not contribute to the equations as their mean value is zero. As stated before, $\langle \hat{b}_n \rangle$ fades and the ansatz leaves $\langle \hat{a}_i \rangle = c_i$ unaffected.

The second order moments will be

$$\langle \hat{a}_i \hat{a}_j \rangle = \langle (c_i + \hat{b}_i)(c_j + \hat{b}_j) \rangle \tag{4.24}$$

This product can be expanded, which gives terms up to second order in $\hat{b}$. Because the quantum fluctuations are assumed small, all equations are worked out up to first order in $\hat{b}$.

Therefore, the time dependence of the operator $\hat{b}_n$ for quantum fluctuations can be constructed by taking the difference of the first and second order mean field equations of motion. This way,

all terms with c_n only will drop out, as they occur in both first and second order mean field. [18] The equations for $\hat{b}_n$ will therefore remain.

After rewriting the equations for two modes, a differential equation for $\hat{b}_1$ and $\hat{b}_2$ can be found in terms of the operators themselves and their complex conjugates. As the equations are worked out to first order in $\hat{b}_n$ and $\hat{b}_n^\dagger$, differential equations for $\hat{b}_n$ and $\hat{b}_n^\dagger$ are linear. For two modes, the system of linear coupled differential equations can therefore be described in a 2x2 matrix B such that

$$\begin{pmatrix} \dot{\hat{b}}_1 \\ \dot{\hat{b}}_1^\dagger \\ \dot{\hat{b}}_2 \\ \dot{\hat{b}}_2^\dagger \end{pmatrix} = B \begin{pmatrix} \hat{b}_1 \\ \hat{b}_1^\dagger \\ \hat{b}_2 \\ \hat{b}_2^\dagger \end{pmatrix} \tag{4.26}$$

The 4x4 matrix B is defined as

$$B = \begin{pmatrix} \alpha & \beta & \gamma & \delta \end{pmatrix} \tag{4.27}$$

With

$$\alpha = \begin{matrix} 4U|c_1|^2 + 2iK_{12}(c_1^* c_2 - c_1 c_2^*) \\ -2Uc_1^{*2} + 2iK_{12}c_1^* c_2^* \\ 2iK_{12}(|c_2|^2 - |c_1|^2) \\ -iK_{12}(c_1^{*2} + c_2^{*2}) \end{matrix} \qquad \beta = \begin{matrix} 2Uc_1^2 + 2iK_{12}c_1 c_2 \\ -4U|c_1|^2 + 2iK_{12}(c_1 c_2^* - c_1^* c_2) \\ -iK_{21}(c_1^2 + c_2^2) \\ 2iK_{12}(|c_2|^2 - |c_1|^2) \end{matrix}$$

$$\gamma = \begin{matrix} 2iK_{12}(|c_1|^2 - |c_2|^2) \\ -iK_{12}(c_1^{*2} + c_2^{*2}) \\ 4U|c_2|^2 + 2iK_{12}(c_1 c_2^* - c_1^* c_2) \\ -2Uc_2^{*2} + 2iK_{12}c_1^* c_2^* \end{matrix} \qquad \delta = \begin{matrix} -iK_{12}(c_1^2 + c_2^2) \\ 2iK_{12}(|c_1|^2 - |c_2|^2) \\ 2Uc_2^2 + 2iK_{12}c_1 c_2 \\ -4U|c_2|^2 + 2iK_{12}(c_1^* c_2 - c_1 c_2^*) \end{matrix}$$

The eigenvalues for the matrix B are determined with Matlab (see Appendix A). For the values of c_1 and c_2, the results from the first order mean field equations of motion are used. These vary in time, and thus will the eigenvalues have a different value for each time instance. However, it can be noted that the eigenvalues are always of the form ai, b, $-ai$ and $-b$, with a and b real and positive. It is important to point out that this result was thus found by filling in various values for $|c_1|^2$ and $|c_2|^2$ at random times, and is not proven mathematically. From this, it can be deduced (with a critical note) that the system of differential equations for $\hat{b}_1$, $\hat{b}_1$, $\hat{b}_1^\dagger$ and $\hat{b}_2^\dagger$ is unstable because one of the eigenvalues has a real part larger than zero.

Therefore, the quantum fluctuations $\hat{b}_n$ cannot be neglected for this two mode system. These results (partly) explain the instability that shows in te solutions of the equations of motion in Section 4.2.

[18] Intuitively, this can be described in the following manner. The equation is not exact however, but can be seen as a guide to show what way the resulting differential equations for $\hat{b}_n$ will appear.

$$\left.\frac{d\langle\hat{a}_n\rangle}{dt}\right|_{\text{mf 2}} - \left.\frac{d\langle\hat{a}_n\rangle}{dt}\right|_{\text{mf 1}} = \frac{dc_n}{dt} + \frac{d\hat{b}_n}{dt} - \frac{dc_n}{dt} = \frac{d\hat{b}_n}{dt} \tag{4.25}$$

. In the equation above, 'mf 1' is for first order and 'mf 2' for second order mean field.

5 Concluding Remarks

First and second order mean field approximations are applied to the equations of motion of the amplitudes $c_n = \langle \hat{a}_n \rangle$ for each mode of an isolated quantum many-body system. In first order mean field, under the assumption that each mode has the same (constant) amplitude, the Kuramoto equation follows for the phases of the complex amplitudes [1]. All correlations between the operators of various modes are neglected in this approximation. To study this and to refine the mean field solution, the equations of motion have been extended to second order mean field.

Numerical integration has been used to solve the system of coupled differential equations for two modes. The solutions showed to be unstable. This was verified by defining quantum fluctuations beyond mean field, which were shown not to be negligible. Possible causes for instability could be the limitation to two modes only, for which the mean field solution might not approximate the system closely enough.

Because of the high frequent oscillations in the amplitudes and the instability of the solutions, comparison between the mean field equations of motion and the Kuramoto model was difficult. Furthermore, no solutions were found which could give some insight in the new approximation of the mean field equations of motion. It can therefore not be concluded what the effect is of extending the mean field approximation to second order, for a set of two modes.

Further research could include a higher number of modes in the numerical integration, to be able to check for the effects of extending to second order mean field. These equations of motion are theoretically determined for an arbitrary number of modes, and can thus be used. Moreover, the use of different integration methods and their stability could be analysed further, as well as the stability of the Kuramoto equations themselves.

References

[1] Dirk Witthaut et al. *Classical synchronization indicates persistent entanglement in isolated quantum systems*. Nature, 2016.

[2] Juan A. Acebrón et al. *The Kuramoto model: a simple paradigm for synchronization phenomena*. Vol. 70. Reviews of Modern Physics, 2005.

[3] Sz Boda et al. *Kuramoto-type phase transition with metronomes*. European Journal of Physics, 2013.

[4] Stephen M. Barnett and Paul M. Radmore. *Methods in Theoretical Quantum Optics*. Oxford University Press, 2003.

[5] Ingemar Bengtsson and Karol Zyczkowski. *Geometry of Quantum States*. Cambridge University Press, 2006, pp. 1–8.

[6] Salomon Bochner and Komaravolu Chandrasekharan. *Fourier Transforms*. Princeton University Press, 1949.

[7] Martin Braun. *Differential Equations and their Applications*. Springer, 1993.

[8] Hayato Chiba and Georgi S. Medvedev. *The mean field analysis for the Kuramoto model on graphs I. The mean field equation and transition point formulas*. Institute of Mathematics for Industry, Kyushu University and Department of Mathematics, Drexel University, 2016.

[9] Gerald Cooray. *The Kuramoto Model*. Uppsala University, 2008.

[10] Luiz Davidovich. *Quantum Optics in Cavities, Phase Space Representations, and the Classical Limit of Quantum Mechanics*. Federal University of Rio de Janeiro, 2000.

[11] R. Demkowicz-Dobrzański, M. Jarzyna and J. Kołodyński. *Quantum limits in optical interferometry*. Progress in Optics, 2014.

[12] Helge Dietert. *Stability and bifurcation for the Kuramoto model*. Elsevier, 2015.

[13] Florian Dorfler and Francesco Bullo. *Synchronization and Transient Stability in Power Networks and Non-Uniform Kuramoto Oscillators*. SIAM Journal on Control and Optimization, 2012.

[14] Peter D. Drummond and Zbignieuw Ficek. *Quantum Squeezing*. Springer-Verlag, 2004.

[15] Jens Eisert and Martin B Plenio. *Focus on Quantum Information and Many-Body Theory*. New Journal of Physics, 2010.

[16] J. Estéve et al. *Squeezing and entanglement in a Bose-Einstein condensate*. Nature, 2008.

[17] Christopher C. Gerry and Peter L. Knight. *Introductory Quantum Optics*. Cambridge University Press, 2005.

[18] Christian Knapp Géza Tóth, Otfried Gühne and Hans J. Briegel. *Optimal Spin Squeezing Inequalities Detect Bound Entanglement in Spin Models*. Physical Review Letters, 2007.

[19] A. Griffin. *Conserving and gapless approximations for an inhomogeneous Bose gas at finite temperatures*. Physical Review Letters, 1996.

[20] David J. Griffiths. *Introduction to Quantum Mechanics*. Cambridge University Press, 1982, pp. 250–292,340–397.

[21] C. Groß. *Spin Squeezing and Non-linear Atom Interferometry with Bose-Einstein Condensates*. Springer, 2012.

[22] Ernst Hairer, Christian Lubich and Gerhard Wanner. *Geometric numerical integration illustrated by the Stormer–Verlet method*. Cambridge University Press, 2003.

[23] Yichen Huang. *Classical simulation of quantum many-body systems.* University of California, Berkeley, 2015.

[24] M. T. Jaekel and S. Reynaud. *Quantum limits in interferometric measurements.* Europhysics Letters, 1990.

[25] Qiqi Wang Karen Willcox. *Computational Methods in Aerospace Engineering.* MIT OpenCourseWare, 2014.

[26] S. Yu. Kourtchatov, V. V. Likhanskii and A. P. Napartovich. *Theory of phase locking of globally coupled oscillators.* Physical Review Letters, 1995.

[27] Araceli Aznar Luque. *The Kuramoto model for Synchronization.* Faculty of Physics, University of Barcelona, 2015.

[28] Jeff Marsh. *The Kuramoto Model, a presentation in partial satisfaction of the requirements for the degree of MSc in Applied Mathematics.* University of Colorado, 2008.

[29] Renato E. Mirollo and Steven H. Strogatz. *The spectrum of the locked state for the Kuramoto model of coupled oscillators.* Elsevier, 2005.

[30] Fernando Parisio. *Coherent-State Overcompleteness, Path Integrals, and Weak Values.* Journal of Mathematical Physics, 2016.

[31] Marlan O. Scully and M. Suhail Zubairy. *Quantum optics.* Cambridge University Press, 1997.

[32] A. Sørensen et al. *Many-particle entanglement with Bose-Einstein condensates.* Nature, 2001.

[33] I. Tikhonenkov, J.R. Anglin and A. Vardi. *Quantum dynamics of Bose-Hubbard Hamiltonians beyond the Hartree-Fock-Bogoliubov approximation: The Bogoliubov back-reaction approximation.* Physical Review Letters, 2007.

[34] Géza Tóth et al. *Spin Squeezing and Entanglement.* Physical Review Letters, 2009.

[35] Loup Verlet. *Computer "Experiments" on Classical Fluids. I. Thermodynamical Properties of Lennard-Jones Molecules.* Physical Review Letters, 1967.

[36] C. Vuik et al. *Numerical Methods for Ordinary Differential Equations.* Delft Academic Press, 2016.

[37] Shinya Watanabe and Steven H. Strogatz. *Constants of motion for superconducting Josephson arrays.* Elsevier Physics, 1994.

[38] Nicholas Wheeler. *Harmonic Oscillator Revisited: Coherent States.* Reed College, 2012.

[39] D. Wineland et al. *Squeezed atomic states and projection noise in spectroscopy.* Physical Review Letters, 1994.

[40] Michael M. Wolf. *Entanglement in Many Body Systems.* Frontiers of Science Symposium, Max-Planck-Institute for Quantum-Optics, 2011.

[41] Michael M. Wolf. *Quantum Many-Body Theory: Divide, perturb and conquer.* Nature, 2008.

[42] Can Xu et al. *Synchronization of phase oscillators with frequency-weighted coupling.* Scientific Reports, 2016.

[43] Dong Yan, Xiao-Guang Wang and Ling-An Wu. *Spin Squeezing and Entanglement of Many-Particle Spin-Half States.* Chinese Physics Letters, 2004.

[44] Wei-Min Zhang, Da Hsuan Feng and Robert Gilmore. *Coherent states: Theory and some applications.* Reviews of Modern Physics, 1990.

A Matlab Code

The first order equations of motion for c_1 and c_2 are implemented in Matlab the following way.

```
function [ dy ] = Ode1( y )
% First order equations of motion for two modes
w=[0.6,0.8];
U=1;
K=1;
dy=zeros(2,1);
dy(1)=(w(1)*y(1)+U*(conj(y(1))*y(1)^2)+K/(2j)*(conj(y(2))*y(1)^2+conj
    (y(2))*y(2)^-2*y(1)*conj(y(1))*y(2)))/1j;
dy(2)=(w(2)*y(2)+U*(conj(y(2))*y(2)^2)+K/(2j)*(conj(y(1))*y(2)^2+conj
    (y(1))*y(1)^-2*y(2)*conj(y(2))*y(1)))/1j;
end
```

The system of coupled differential equations for the second order mean field approximation is implemented in Matlab the following way. These equations are the equations (4.3) and (4.16) - (4.19) defined for both modes.

```
function [ dy ] = Ode2( y )
%UNTITLED Summary of this function goes here
%   Detailed explanation goes here
w=[0.6,0.8];
U=0.5;
K=0.5;
dy=zeros(9,1);
dy(1)= (w(1)*y(1)...
+U*(conj(y(1))*y(3)+2*y(1)*y(6)-2*conj(y(1))*y(1)^2)...
+K/(2j)*(2*y(2)*y(7)-2*y(2)*y(6)...
+2*y(1)*y(9)-2*y(1)*y(8)...
+conj(y(2))*y(4)+conj(y(2))*y(3)-2*conj(y(1))*y(5)...
-2*y(2)^2*conj(y(2))-2*y(1)^2*conj(y(2))+4*y(1)*y(2)*conj(y(1))))/1j;
dy(2) = (w(2)*y(2)...
+U*(conj(y(2))*y(4)+2*y(2)*y(7)-2*conj(y(2))*y(2)^2)...
+K/(2j)*(2*y(1)*y(6)-2*y(1)*y(7)...
+2*y(2)*y(8)-2*y(2)*y(9)...
+conj(y(1))*y(3)+conj(y(1))*y(4)-2*conj(y(2))*y(5)...
-2*y(1)^2*conj(y(1))-2*y(2)^2*conj(y(1))+4*y(2)*y(1)*conj(y(2))))/1j;
dy(3) = (2*w(1)*y(3)...
+U*(2*conj(y(1))*y(3)+4*y(1)*y(6)-4*y(1)^2*conj(y(1)))...
+K/(2j)*(2*y(4)*y(9)+6*y(3)*y(9)-4*y(3)*y(8)...
+4*y(7)*y(5)-8*y(6)*y(5)...
-4*conj(y(2))*y(2)^2*y(1)-4*conj(y(2))*y(1)^2 ...
+8*conj(y(1))*y(2)*y(1)^2))/1j;
dy(4) = (2*w(2)*y(4)...
+U*(2*conj(y(2))*y(4)+4*y(2)*y(7)-4*y(2)^2*conj(y(2)))...
+K/(2j)*(2*y(3)*y(8)+6*y(4)*y(8)-4*y(4)*y(9)...
+4*y(6)*y(5)-8*y(7)*y(5)...
-4*conj(y(1))*y(1)^2*y(2)-4*conj(y(1))*y(2)^2 ...
```

```
+8*conj(y(2))*y(1)*y(2)^2))/1j;
dy(5) = (w(1)*y(5)+w(2)*y(5)...
+U*(y(9)*y(4)+y(8)*y(3)+2*y(5)*y(7)+2*y(5)*y(6)...
-2*y(1)^2*y(2)*conj(y(1))-2*y(1)*y(2)^2*conj(y(2)))...
+K/(2j)*(2*y(7)*y(4)-2*y(6)*y(4)...
+2*y(9)*y(5)-4*y(8)*y(5)...
+y(7)*y(4)+y(7)*y(3)...
-2*y(2)^3*conj(y(2))-2*y(1)^2*y(2)*conj(y(2))+4*y(1)*y(2)^2*conj(y(1))...
+K/(2j)*(2*y(6)*y(3)-2*y(7)*y(3)...
+2*y(8)*y(5)-4*y(9)*y(5)...
+y(6)*y(4)+y(6)*y(3)...
-2*y(1)^3*conj(y(1))-2*y(1)*y(2)^2*conj(y(1))+4*y(1)^2*y(2)*conj(y(2)))/1j;
dy(6) = (U*(conj(y(1))*y(3)+2*y(1)*y(6)...
-2*conj(y(1))*y(6)-y(1)*conj(y(3))...
-2*conj(y(1))*y(1)^2+2*conj(y(1))^2*y(1))...
+K/(2j)*(2*y(9)*y(7)+2*y(8)*y(7)...
-2*y(9)*y(6)-2*y(8)*y(6)...
-2*conj(y(3))*y(5)+2*conj(y(4))*y(5)...
-conj(y(5))*y(3)+conj(y(5))*y(4)...
-2*conj(y(2))^2*y(1)*y(2)+2*conj(y(1))^2*y(1)*y(2)...
-2*conj(y(1))*conj(y(2))*y(2)^2+2*conj(y(1))*conj(y(2))*y(1)^2))/1j;
dy(7) = (U*(conj(y(2))*y(4)+2*y(2)*y(7)...
-2*conj(y(2))*y(7)-y(2)*conj(y(4))...
-2*conj(y(2))*y(2)^2+2*conj(y(2))^2*y(2))...
+K/(2j)*(2*y(8)*y(6)+2*y(9)*y(6)...
-2*y(8)*y(7)-2*y(9)*y(7)...
-2*conj(y(4))*y(5)+2*conj(y(3))*y(5)...
-conj(y(5))*y(4)+conj(y(5))*y(3)...
-2*conj(y(1))^2*y(2)*y(1)+2*conj(y(2))^2*y(2)*y(1)...
-2*conj(y(2))*conj(y(1))*y(1)^2+2*conj(y(2))*conj(y(1))*y(2)^2))/1j;
dy(8) = (-w(1)*y(8)+w(2)*y(8)...
+U*(-conj(y(3))*y(5)-2*y(6)*y(8)...
+conj(y(5))*y(4)+2*y(8)*y(7)...
+2*conj(y(1))^2*y(1)*y(2)-2*conj(y(1))*conj(y(2))*y(2)^2)  ...
+K/(2j)*(2*y(7)*y(7)-2*y(7)*y(6)...
+2*y(9)*y(9)-2*y(9)*y(8)...
+y(4)*conj(y(4))+y(3)*conj(y(4))-2*y(5)*conj(y(5))...
-2*conj(y(2))^2*y(2)^2-2*conj(y(2))^2*y(1)^2+4*conj(y(1))*conj(y(2))*
    y(1)*y(2))...
+K/(2j)*(2*y(6)*y(6)-2*y(6)*y(7)...
+2*y(9)*y(9)-2*y(9)*y(8)...
+y(3)*conj(y(3))+y(3)*conj(y(4))-2*y(5)*conj(y(5))...
-2*conj(y(1))^2*y(1)^2-2*conj(y(2))^2*y(1)^2+4*conj(y(1))*conj(y(2))*
    y(1)*y(2)))/1j;
dy(9) = (-w(2)*y(9)+w(1)*y(9)...
+U*(-conj(y(4))*y(5)-2*y(7)*y(9)...
+conj(y(5))*y(3)+2*y(9)*y(6)...
```

```
+2*conj(y(2))^2*y(2)*y(1)-2*conj(y(2))*conj(y(1))*y(1)^2)  ...
+K/(2j)*(2*y(6)*y(6)-2*y(6)*y(7) ...
+2*y(8)*y(8)-2*y(8)*y(9) ...
+y(3)*conj(y(3))+y(4)*conj(y(3))-2*y(5)*conj(y(5)) ...
-2*conj(y(1))^2*y(1)^2-2*conj(y(1))^2*y(2)^2+4*conj(y(2))*conj(y(1))*
    y(2)*y(1)) ...
+K/(2j)*(2*y(7)*y(7)-2*y(7)*y(6) ...
+2*y(8)*y(8)-2*y(8)*y(9) ...
+y(4)*conj(y(4))+y(4)*conj(y(3))-2*y(5)*conj(y(5)) ...
-2*conj(y(2))^2*y(2)^2-2*conj(y(1))^2*y(2)^2+4*conj(y(2))*conj(y(1))*
    y(2)*y(1)))/1j;

end
```

The code to solve these equations is included below.

```
clear all
close all

tmax=100;

% first order
y01=2j*ones(2,1);
[t1,y1]=ode45(@(t,y1)Ode1(y1), [0 tmax], y01);  %or ode23t
plot(t1,angle(y1(:,1)))
hold on
plot(t1,angle(y1(:,2)),'r')
h1=legend('$\phi_1$','$\phi_2$');
xlabel('Time $t$','Interpreter','Latex','Fontsize',15)
ylabel('Phase $\phi_i$ of complex amplitude $c_i$','Interpreter','
    Latex','Fontsize',15)
set(h1, 'Interpreter', 'latex','Fontsize', 15)
figure
plot(t1,abs(y1(:,1)));
hold on
plot(t1,abs(y1(:,2)),'r');
h2=legend('$|c_1|^2$', '$|c_2|^2$');
set(h2, 'Interpreter', 'latex','Fontsize',15)
xlabel('Time $t$','Interpreter','Latex','Fontsize',15)
ylabel('Magnitude complex amplitude $|c_i|^2$','Interpreter','Latex',
    'Fontsize',15)

%% second order
y02=2j*ones(9,1)*2j;
[t2,y2]=ode45(@(t,y2)Ode2(y2), [0 tmax], y02);  %or ode23t
figure
plot(t2,angle(y2(:,1)),'b')
hold on
plot(t2,angle(y2(:,2)),'r')
```

```
h1=legend('$\phi_1$','$\phi_2$');
xlabel('Time $t$','Interpreter','Latex','Fontsize',15)
ylabel('Phase $\phi_i$ of complex amplitude $c_i$','Interpreter','
    Latex','Fontsize',15)
set(h1, 'Interpreter', 'latex','Fontsize', 15)
print -djpeg90 phasesecondorder.jpg

figure
plot(t2,abs(y2(:,1)),'b');
hold on
plot(t2,abs(y2(:,2)),'r');
h2=legend('$|c_1|^2$', '$|c_2|^2$');
set(h2, 'Interpreter', 'latex','Fontsize',15)
xlabel('Time $t$','Interpreter','Latex','Fontsize',15)
ylabel('Magnitude complex amplitude $|c_i|^2$','Interpreter','Latex',
    'Fontsize',15)

%% matrix
clc
tpoint = 0.5*tmax;                          %moment in time for
    determining matrix element
n1 = round(tpoint*(length(t1)/tmax));   %index of element at t=tpoint
n2 = round(tpoint*(length(t2)/tmax));
c1=y1(n1,1);
c2=y1(n1,2);
w=[0.6,0.8];
U=0.5;
K=0.8;
matrix = 1/1j*[4*U*abs(c1)^2+2j*K*(conj(c1)*c2-c1*conj(c2)),2*U*c1
    ^2+2j*K*c1*c2,...
2j*K*(abs(c1)^2-abs(c2)^2), -1j*K*(c1^2+c2^2);...
-2*U*conj(c1)^2+2j*K*conj(c1)*conj(c2), -4*U*abs(c1)^2+2j*K*(c1*conj(
    c2)-conj(c1)*c2),...
-1j*K*(conj(c1)^2+conj(c2)^2), 2j*K*(abs(c1)^2-abs(c2)^2);...
2j*K*(abs(c2)^2-abs(c1)^2), -1j*K*(c1^2+c2^2), 4*U*abs(c2)^2+2j*K*(c1
    *conj(c2)-conj(c1)*c2),...
2*U*c2^2+2j*K*c1*c2;...
-1j*K*(conj(c1)^2+conj(c2)^2),2j*K*(abs(c2)^2-abs(c1)^2), -2*U*conj(
    c2)^2+2j*K*conj(c1)*conj(c2),...
-4*U*abs(c2)^2+2j*K*(conj(c1)*c2-c1*conj(c2))];
e=eig(matrix);
```